POLITECNICO DI TORINO

Master's Degree in Nanotechnologies for ICTs

Master's Degree Thesis

Study of buffer ion concentration in fast-scan cyclic voltammetry method using nano-graphitic sensors

Supervisors

Prof. Davood Shahrjerdi

Prof. Matteo Cocuzza

Candidate

Edoardo Lombardi

October 2023

Summary

Point-of-Care diagnostic and implantable devices have been on the rise over the last twenty years due to their numerous benefits in healthcare delivery. In this context, nano-graphitic carbon sensors, along with other types of carbon-based sensors, have emerged as optimal candidates, because they can be assembled into densely packed arrays of microelectrochemical sensors with high performance in neurotransmitters detection.
The fast-Scan cyclic voltammetry method is one of the best-known methods for measuring electrochemically active neurotransmitters. One of the important aspects of electrochemical measurements is the buffer solution used in the electrochemical sensing of neurotransmitters. However, the effect of the buffer solution has not yet been studied in FSCV measurements. The aim of this thesis is to investigate how buffer concentration can affect the characteristics of neurotransmitters such as sensitivity or impedance of the sensors.
Several experiments were performed in which bioanalytes with different characteristics (dopamine, serotonin and melatonin) were dissolved in a buffer solution (phosphate-buffered saline), varying the concentration of the latter. These measurements were performed with the fast-scan cyclic voltammetry technique and using a custom-made experimental apparatus. The sensor was combined with an integrated readout circuit. The current signal was measured and then digitised using a data acquisition instrument. The results were extracted and analysed with custom-made programs. With this work, the understanding of the electrochemical behaviour of neurotransmitters during sensing experiments can be improved for future applications.

Acknowledgements

I would like to express my sincere gratitude and appreciation to all those who have contributed to the successful completion of this master thesis.
First and foremost, I am deeply indebted to my supervisors, Prof. Davood Shahrjerdi and Moeid Jamalzadeh, for their guidance, support and insightful feedback throughout this research journey. Their expertise and help have been instrumental in shaping the direction of this study. At the same time I cannot avoid to thank also the other students that have shared with me the laboratory and also helped me in this project.
Besides the thesis, my profound thanks go also to all my friends, the ones I met during these university years, the ones from my home town and especially the ones I grew up with, all of them have been a constant source of motivation and companionship.
Finally, I cannot overlook the support and encouragement of my family, whose love and belief in me have been the pillars of my growth. Your sacrifices and understanding during the challenging times of this journey are deeply appreciated.
In conclusion, this work stands as a testament to the collaborative efforts and support from all those around me. Your contributions, big and small, have played a crucial role in the completion of this master thesis, and I am truly grateful for each one of you.

Thank you all.
Edoardo

Table of Contents

List of Tables

List of Figures

Acronyms

5HT
Serotonin

ATM
Atomic force microscopy

CTE
Coefficient of thermal expansion

DA
Dopamine

DoQ
Dopamine-ortho-quinone

EBL
Electron-bean lithography

EIS
Electrochemical Impedance Spectroscopy

FSCV
Fast-scan cyclic voltammetry

IC
Integrated circuit

LPL
Lower potential limit

MT

Melatonin

NG

Nano-graphitic

PBS

Phosphate buffered saline

RMS

Root-mean-square

RPS

Rapid potential sweep

SBR

Signal to background ratio

SPS

Slow potential sweep

UHV

Ultra-high vacuum

UPL

Upper potential limit

Chapter 1

Introduction

In recent decades, electrochemical sensors have been extensively researched as a useful tool in the context of point-of-care diagnostic and implantable devices, as they can provide numerous benefits in healthcare delivery. In particular, carbon materials are biocompatible, possess rich surface chemistry, a favourable electrochemical activity and high resistance to bio-fouling, making them an optimal choice for building electrochemical sensors. Another desirable outcome in biomolecule detection is the implementation of a large-scale sensing system consisting of multiple microscopic, carbon electrodes packed in close proximity to each others. In addition, these sensors made out of carbon materials should also be capable of having an adjustable temporal resolution, which is particularly useful for measurements in complex biological systems, where the temporal dynamics of the bioanalytes can vary greatly. An example of this behaviour is the fluctuation of dopamine (DA) inside the brain. In the tonic mode (the extracellular level of the baseline DA), slow changes occur over the course of minutes and hours, whereas fluctuations in the phasic mode are of the order of a few seconds [1, 2, 3]. Sensors made of thin-film carbon materials with a graphitic structure have emerged as a possible solution that has all the above properties [4].

It is also important to mention that the content of bioanalytes in a biological system can be remarkably low, for example, in the case of phasic and tonic DA it is in the order of 10nM and 100nM [5, 6, 7, 8]. It is known that the sensitivity of nano-graphitic (NG) sensors is influenced by defects and functional groups on their surface. For this reason, another important research focus is the development of units with higher sensitivity to the presence of bio-analytes. This type of approach has an upper physical limit, which is reached when the spatial density of the defects becomes too high and the material is converted into completely disordered carbon. A second type of sensitivity improvement is achieved by optimising the detection integrated circuit (IC) and the waveform used in fast-scan cyclic voltammetry (FSCV) measurements [9]. The changes in the signal lead to an increased number

of adsorbed molecules and thus to a higher output signal. Another factor that can influence the sensitivity of the sensor is the choice of buffer solution used.
The chemical composition of these solutions can be the cause of this influence and it is possible to have a change in sensitivity caused by a variation in the ion concentration of the buffer. For this reason, several experiments were conducted to determine how a change in the ion concentration of a common buffer solution, phosphate buffered saline (PBS), could affect the sensitivity of the NG sensors. The experiments used the FSCV technique, in which the redox current resulting from the presence of a neurotransmitter was extracted from the total signal by subtracting the background current originating from the sensor. The optimised waveforms were used to detect the bioanalytes, while the traditional waveform was chosen to record the background current. In addition to the study of the variation of the sensitivity, some observations of the capacitive response of the sensors were also conducted in order to see the influence on the impedance of the sensors.
The procedure for developing the electrochemical sensing units, as determined by previous studies, is reported first, followed immediately by a description of their properties. After this first part, the techniques used to perform the measurements and the deviations from conventional FSCV standards are described, as well as a description of the experimental apparatus setup. The third and final part of this work deals with the results obtained and their significance. In particular, it will be shown how the different buffer ion concentrations can lead to different type of behaviours when detecting some bio-analytes on the sensor surface, depending on the chemical characteristics of the latter ones.

Chapter 2

The electrochemical sensing unit

2.1 The nano-graphitic microsensor

Carbon materials are widely used for biomolecule detection due to their various properties such as biocompatibility, rich surface chemistry, favourable electrochemical activity and strong resistance to bio-fouling. In addition, the implementation of a large-scale sensing system consisting of multiple microscopic, closely packed carbon electrodes is the goal of biomolecule detection applications. One promising way to achieve this is to fabricate thin-film carbon materials on top of dielectric-coated substrates using standard microfabrication techniques.
Once the sensor is fabricated, the output signal must be amplified and digitised by the IC and the combination of the sensor and detection circuit forms the complete electrochemical sensing unit.
This biochip family can perform parallel measurements that can be used in a variety of applications, such as point-of-care diagnostics [10] or in the study of chemical signals in living cells [11].

2.1.1 Synthesis of the nano-graphitic sensor

The first thing to choose is the type of substrate. In this case, it is a dielectric-coated silicon one, because it is inexpensive, available in large dimensions and compatible with standard microfabrication techniques. The disadvantage of the silicon substrate is that its thermal stability limits the production temperature to 1100°C, resulting in a material with a completely disordered sp^2 structure and consequently slow electron transfer kinetics and poor sensing properties [12, 13]. To achieve fast electron transfer kinetics, it is desirable that the resulting thin-film

materials have graphitic structures instead. The process to achieve this is often referred to as metal-induced graphitisation and consists of a high-temperature thermal treatment (pyrolysis [12, 14, 15, 16, 17, 18, 19, 20]) performed in the presence of a metal catalyst (such as nickel) that promotes the solid-state conversion of amorphous carbon to graphene [21].

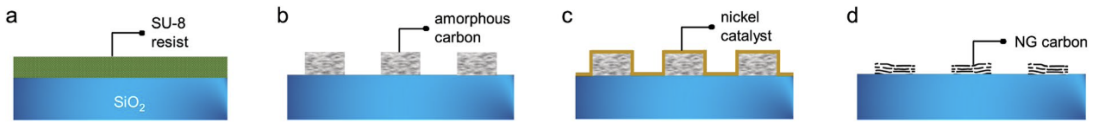

Figure 2.1: Schematic illustration of the main steps of the micro-scale NG carbon islands synthesis [4]

The starting point of the fabrication is the thermally grown SiO_2 substrate onto which the SU-8 resist material is deposited (2.1a). The successive generation of the amorphous carbon islands is carried out in a two-step process. First, the resist is broken down into islands with the correct shapes and dimensions using electron beam lithography (EBL). Then the SU-8 islands are annealed in a non-oxidising environment at 450°C to induce their carbonisation (2.1b). The resulting islands consist of an amorphous sp^2 hybridised carbon [22, 23, 24] that is converted into the desired NG carbon material by metal-induced graphitisation. This final process involves two main steps, the deposition of an ultra-thin (sub-2nm) nickel film as a metal catalyst in an ultra-high vacuum (UHV) environment (2.1c), followed by the annealing of the sample at 1100°C (2.1d).

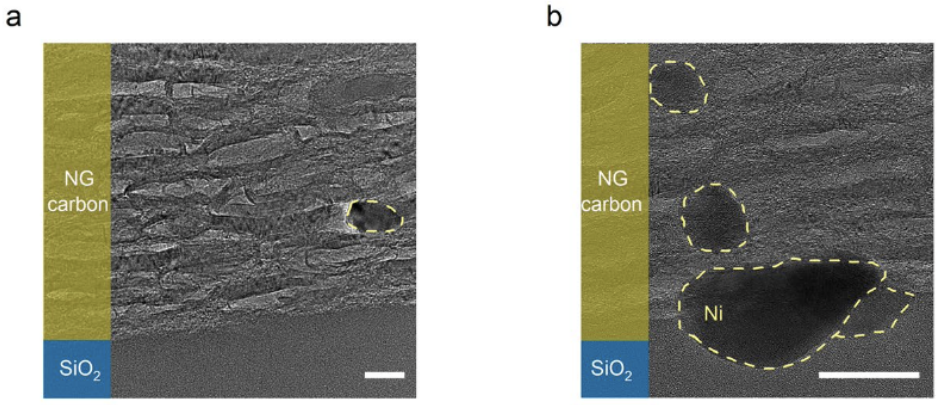

Figure 2.2: Cross-section TEM images of a NG carbon film on SiO_2 at different magnifications [4]

The thickness of the catalyst was chosen in order to have a certain density of

structural defects in the resulting material, which determines the sensitivity and the charging current of the electrochemical sensor [13, 25, 26, 27, 28, 29, 30, 31, 32, 33, 34, 35].
Two things can be observed: the nickel is segregated near the SiO_2 interface in the form of nanoparticles (2.2b) [36] and there is a preferential orientation of the graphitic planes that is parallel to the substrate (2.2a). This second property is obtained by applying in-plane tensile strain to the islands during heat treatment and this strain is achieved by relying on the adhesion of the island to the substrate and on the mismatch in the coefficient of thermal expansion (CTE) between them [37, 38].

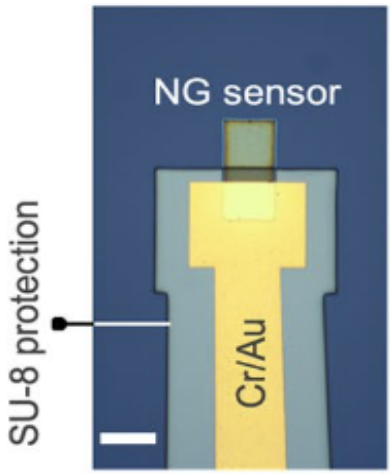

Figure 2.3: NG microsensor optical image [4]

Finally, the microsensors are fabricated using standard microfabrication techniques. The low-resistance Cr/Au metal contacts are obtained with a combination of EBL, e-beam evaporation and lift-off. EBL is then used to pattern the SU-8 resist in order to define the area of the sensor and to prevent the metal contacts from being touched by the solution during the *in vitro* experiments [4].

2.1.2 Structural properties

It has already been mentioned that the characteristics of the sensor depend on its structural properties. In order to optimise the fabrication, different studies were conducted. Raman spectroscopy was used to estimate the density of structural defects on the sensor surface [39]. In particular, by analysing the G and D peaks (2.4), it was possible to determine the average density of point defects ($n_{0D} = 1/L_D^2$) and the average graphitic crystallite size (L_a^2), where L_D and L_a are the average distance between point defects and between line defects, respectively. Furthermore,

the shape of the G and 2D peaks (2.4) confirmed that the NG films were on stage (i) of the graphene amorphisation trajectory and far from stage (ii) of it [40, 41].

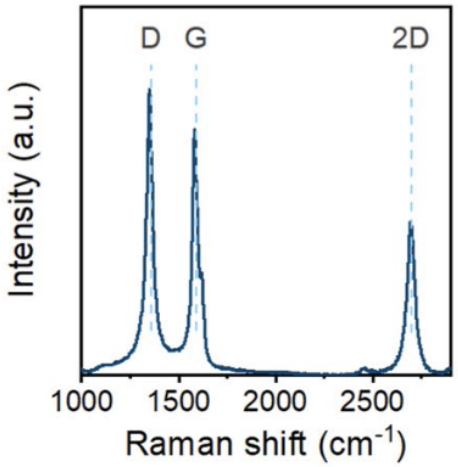

Figure 2.4: Raman spectrum of a NG microsensor [4]

Once the defects were quantified, it was possible to determine their influence on the redox and background currents of the sensors. The results were obtained by normalising them to the DA concentration and to the surface area. This one was determined using only the geometric area, as the root-mean-square (RMS) was less than $10nm$ (2.5).

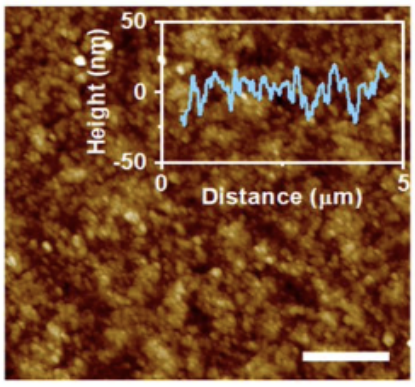

Figure 2.5: AFM topographic image of a NG microsensor [4]

The results showed that the sensitivity was not affected by the crystallite size, but instead increased linearly with the average density of the point defects. It appears

that each point defect promotes adsorption and electron transfer and thus, it act as a single active electrochemical site, increasing the FSCV sensitivity of DA (2.6) [4]. Another important value was the signal to background current ratio (SBR), which was evaluated by taking into account the "intrinsic" background current, i.e. the current obtained by removing the effect of the parasitic background current (caused by the coupling between the substrate and the metal contact of the sensor [19]) from the measured current.

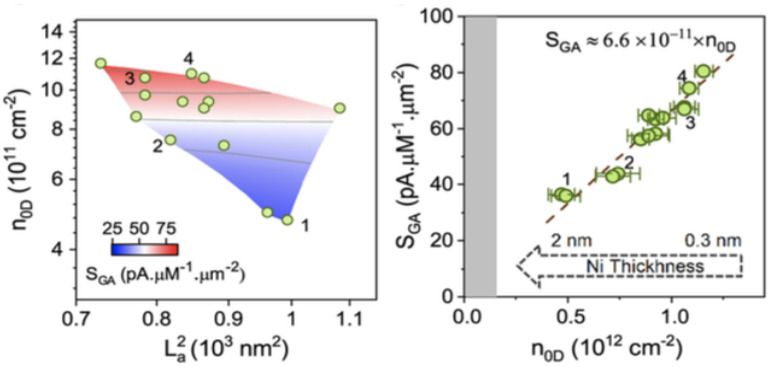

Figure 2.6: Relations between S_{GA} (sensitivity per unit area), L_a^2 and n_{0D} [4]

It has been observed that the SBR does not grow correspondingly when the S_{GA} is increased. This was because the number of point defects also determined an increase in the capacitance of the material in an ionic solution and the intrinsic background current is proportional to the magnitude of this capacitance. Besides the point defects, other factors also determine the amplitude of the background current and thus the SBR, as point defects alone are not sufficient to explain the exact fluctuations in the data. On the other hand, it could be seen that the SBR increased monotonically with the average size of the graphitic crystallites (2.7).

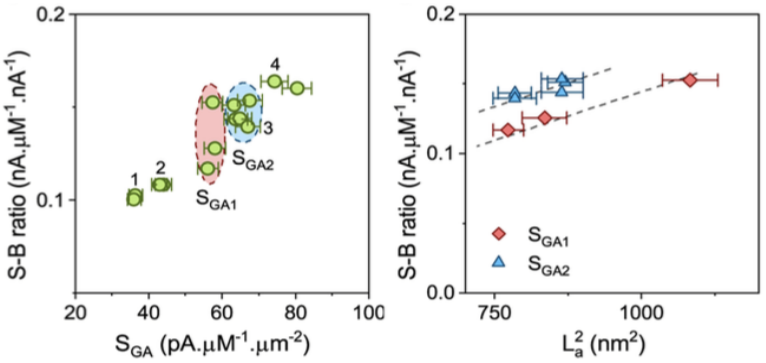

Figure 2.7: Relations between S_{GA}, L_a^2 and SBR [4]

This can be attributed to a reduction in sensor capacitance and thus of the background current. In particular, the experimental results showed how the apparent capacitance (C_{app}), i.e. the capacitance normalised to the area of the sensor, decreased as the crystallite sizes increased for a given density of point defects.
It is important to have a higher signal-to-noise ratio and thus a better SBR to increase the sensitivity of the sensor. The model presented corresponded to a linearly increasing SBR with respect to the defect ratio (D.R.), with $D.R. = n_{0D}/N_{CD}$ and $N_{CD} = \frac{L_a^2}{3} + L_D^2$, leading to the conclusion that maintaining a high density of point defects while increasing the graphitic crystallite size will produce sensors with an improved detection limit (2.8) [4].

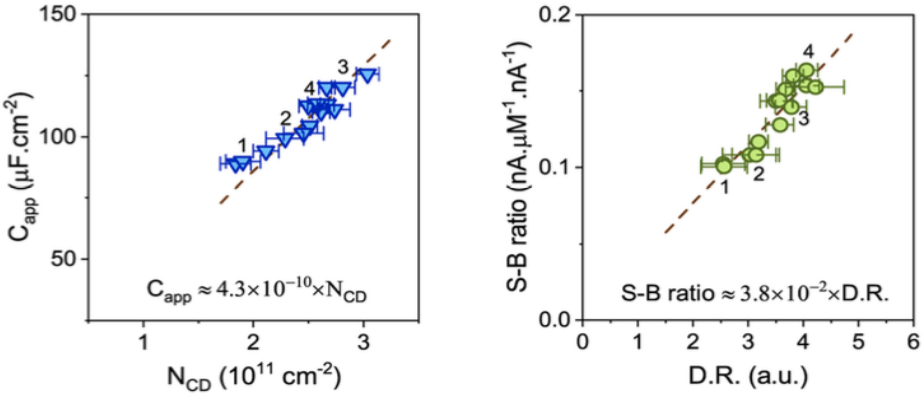

Figure 2.8: Relations between C_{app}, SBR and defect densities (N_{CD} and D.R.) [4]

2.2 The detection circuit design concept

The other part of the electrochemical sensor is the detection IC. This one is fundamental for measuring the bioanalyte concentration using the redox current and the background current generated by the sensor.
Sensors can operate over a range of a few mV/s to hundreds of mV/s, and the operating region of the circuit must be chosen accordingly. When working with a slow potential sweep (SPS), the IC must operate in weak inversion, while for experiments with rapid potential sweep (RPS), strong inversion is required due to the high temporal resolution required. Also to be considered are the dimensions of the sensor, which were built with a geometric area of less than $625\mu m^2$, and finally the noise requirements to detect the lowest possible concentrations (about 10nM for RPS and 100nM for SPS) [42].
Once built, the biochip can maintain the required performance, while being configured for optimal power consumption as needed, depending on the temporal

resolution requirements of the sensing experiments. Another important feature of the IC was the ability to perform parallel multichannel measurements on different sensors. The use of CMOS technology for building this type of circuits is what made possible to have electrochemical biochips with superior capabilities, that consume lees power and have a smaller footprint on top of providing better performances.

Chapter 3

Methods

3.1 Fast-scan cyclic voltammetry for neurotransmitters detection

FSCV is an electrochemical method for detecting and measuring the concentration of neurotransmitters, such as DA, in real time. FSCV is widely used to study the dynamics of neurotransmitter release and uptake in the brain. A special microelectrode made of carbon material is used as the working electrode. This one is inserted into the region of interest, such as the specific brain region where release is expected.
In this measurement technique, a fast voltage sweep is applied to the electrode. As the voltage is cycled, the analyte is oxidized and reduced on the electrode surface. During oxidation, it loses electrons; during reduction, it gains electrons. These electron transfers produce characteristic electrochemical signals that can be measured with the FSCV setup. The current flowing in response to oxidation and reduction is then recorded by the system. The resulting I-V waveform, known as the cyclic voltammogram, shows characteristic peaks that correspond precisely to a particular bio-analyte.
Before FSCV can be used for *in-vivo* detection, a calibration step is required. This involves measuring the current response to known concentrations of an analyte to establish a relationship between the current signal and its concentration. The calibration curve is then used to convert the currents recorded during the experiments to their concentration values.
FSCV allows researchers to monitor the concentration changes of neurotransmitters in real time during different experimental conditions or behavioral tasks. It provides valuable insights into the dynamics of their release and their role in various brain functions. It is an indispensable tool for neuroscientists studying chemical signaling in the brain and can be used in various research areas, including addiction,

learning, memory, neuropsychiatric disorders and more. It also offers high temporal resolution, allowing researchers to detect rapid changes in levels associated with specific events or stimuli.

3.1.1 Cyclic voltammetry

As anticipated, the electrochemical sensing technique used for the sensing system is based on the use of cyclic voltammetry.
The currents measured are those that result from the use of a linearly varying potential applied to the sensor (3.1a). The use of a time linear potential sweep facilitates the generation of the cyclic voltammograms from the measured data and also provides the ability to adjust the temporal resolution of the measurements by varying the repetition rate of the potential waveform. This technique also leads to an undesirable result, which is the generation of a background current signal. This is the sum of two contributions, the charge and discharge of the sensor capacitance in an ionic solution and the pseudocapacitance, related to the electrochemical interactions of the ionic solution with the redox-active species on the sensor surface (e.g., quinone-like species) (3.1b) [43].

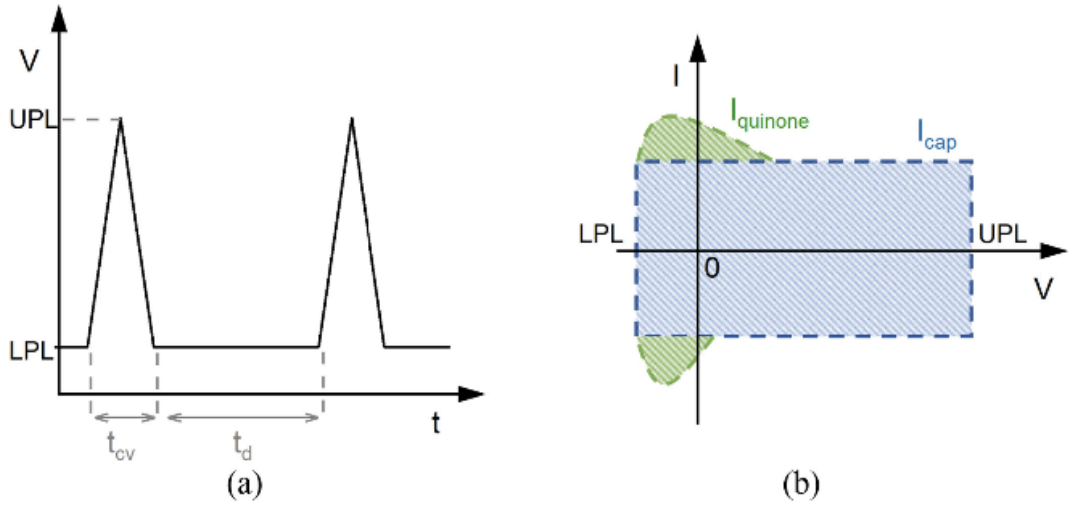

Figure 3.1: Schematic of a triangular potential waveform and of the resulting I-V characteristic of the background current [42]

The presence of a bioanalyte provides another contribution to the resulting overall signal, a redox current, which is the signal of interest and it is much smaller than the background one(3.2) [42]. Another aspect to consider is that the larger the background current, the stronger the noise of the measurement, so that the limit for the lowest detectable concentration becomes more stringent [10, 44, 45].

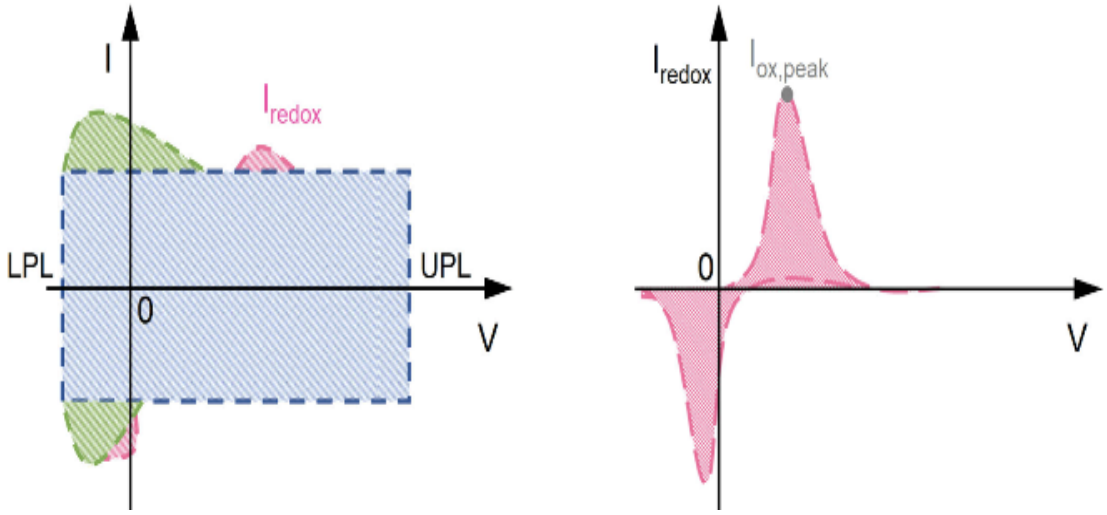

Figure 3.2: Total signal with a bio-analyte in the solution and final voltammogram [42]

The I_{cap} is defined as the sensor capacitance times the sweep rate. Consequently, this limitation is particularly significant when measuring low concentrations of bioanalytes using RPS. It has been observed that the scaling of the potential sweep rate affects both the amplitude of the background current (I_{cap}) and the redox current (I_{redox}). While the amplitude of I_{cap} increases linearly with the potential sweep rate, the amplitude of I_{redox} is affected in different ways depending on whether the measurement is made at a RPS or a SPS. When the potential sweep rate is large enough, the redox reaction is adsorption-limited [46] and a delay time (t_d) is introduced to increase the adsorption of the analyte and thus the amplitude of I_{redox}. If t_d is chosen accurately, I_{redox} also increases linearly with the potential sweep rate. The S-B ratio, defined as $I_{ox,peak}/I_{cap}$, remains constant but is typically smaller than in the SPS case. Another consideration is that the digitization error of the detection circuit is a bigger problem when detecting bio-analytes in RPS because the background current is much larger.
When extracting I_{redox} from the total current, it is also important to consider that the background current is not time-invariant, but changes in an unpredictable manner. When measuring low-concentrations of bioanalytes, an optimal solution is to record the overall shape of the background current and then use it in the analysis. The final I_{redox} shape is obtained by simply subtracting the recorded background current from the total signal. The need to subtract the background means that FSCV is an inherently differential technique and is therefore well suited for measuring rapid changes in neurotransmitter levels.

3.1.2 Measurement setup

The *in vitro* measurement setup consists of the flow chamber, the injection pumps, the electronic board as interface and an external computer (3.3a).

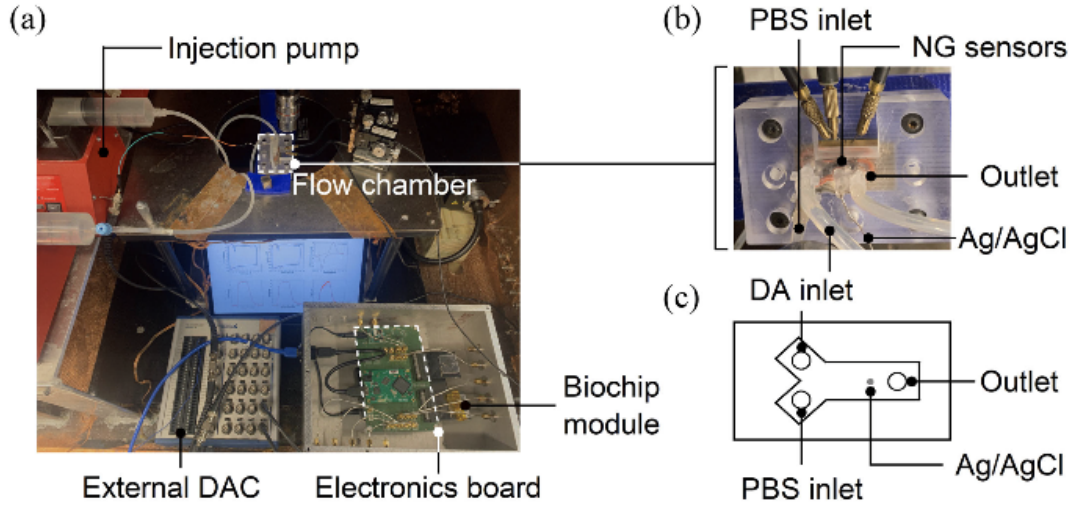

Figure 3.3: Detailed *in vitro* measurement setup and microfluidic chamber [42]

A custom-made microfluidic chamber with two inlets and one outlet in a Y-shape was used, which also housed the Ag/AgCl reference electrode (3.3c).
Due to the low currents of the microsensor, a two-electrode scheme was deemed appropriate. The connection between the sensor and the detection IC was made by some micromanipulator probes (3.3b) [34].

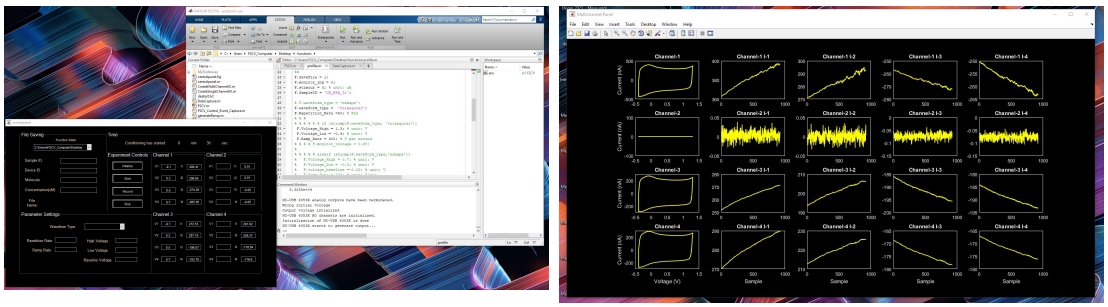

Figure 3.4: Custom-made program for data extraction

Finally, a customised program was developed in MATLAB for recording and analysing the data (3.4).

3.1.3 Measurement optimizations

Dopamine detection

It has been said that in experiments under a RPS, one way to increase the number of bioanalyte molecules absorbed on the sensor surface, and thus the sensitivity, is to incorporate a hold time. As an undesirable consequence, the temporal resolution is reduced. Since DA is a positively charged molecule, it has also been shown that its adsorption on the sensor surface is enhanced by electrostatic attraction when the potential applied during t_d is held at a more negative value [47, 48].
In FSCV measurements using a conventional waveform, the potential is scanned from a negative to a positive value and back to the initial value, oxidising DA to Dopamine-ortho-quinone (DoQ) during the forward scan and reducing it back during the reverse scan. The upper and lower potential limits (UPL and LPL) must be carefully selected to include the full shape of the oxidation and reduction peaks of the bioanalyte.

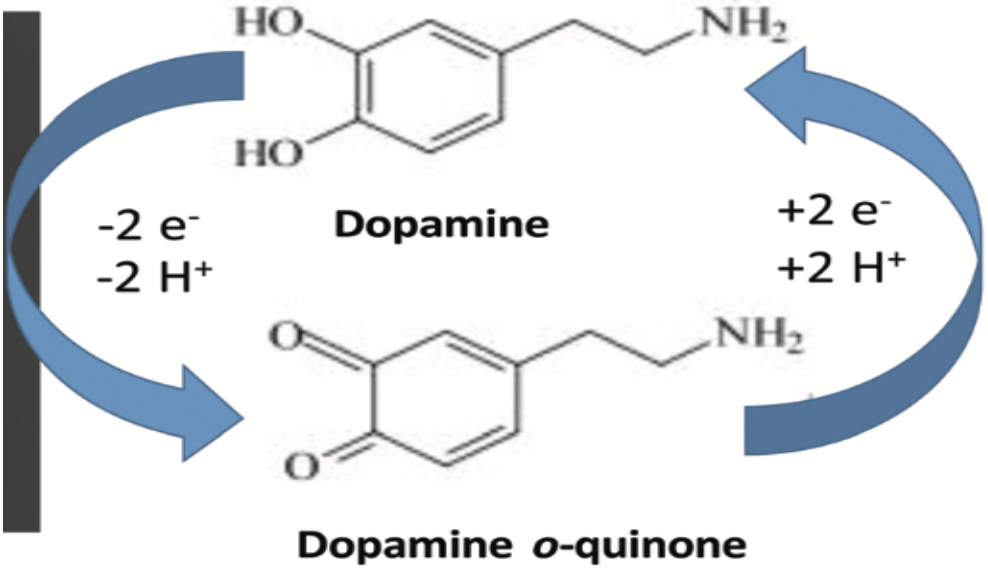

Figure 3.5: DA redox reaction [48]

The starting point for waveform optimization was the traditional triangular waveform, where the potential was scanned from -0.4V to 1.3V with a frequency of 10 Hz at 400Vs^{-1}. The frequency was chosen so that t_d at the holding potential would be long enough to achieve good DA adsorption on the surface before being rapidly stripped for detection. The negative value for the holding potential arises for two reasons: the value must be negative to attract positively charged DA molecules and it must be low enough to capture the entire reduction peak. At the same time, it must not be too negative, since oxygen begins to reduce at -0.6V, producing

radical byproducts. Similarly, the positive value must be high enough to include the oxidation peak, but not too high to avoid water oxidation (1.5V). Finally, the value of the scan rate resulted from a compromise between being large enough to obtain good stable currents (DA adsorption increases linearly with the scan rate) without being so high as to distort the peak and make them spread to higher potential values [48].
With respect to this conventional waveform, an earlier study of the NG sensor used for this work showed how its shape can be changed to increase the sensitivity. The first parameter varied was the UPL. A decrease in the UPL had no visible effect on the background shape, while the peak oxidation and reduction currents were greatly increased (3.6).

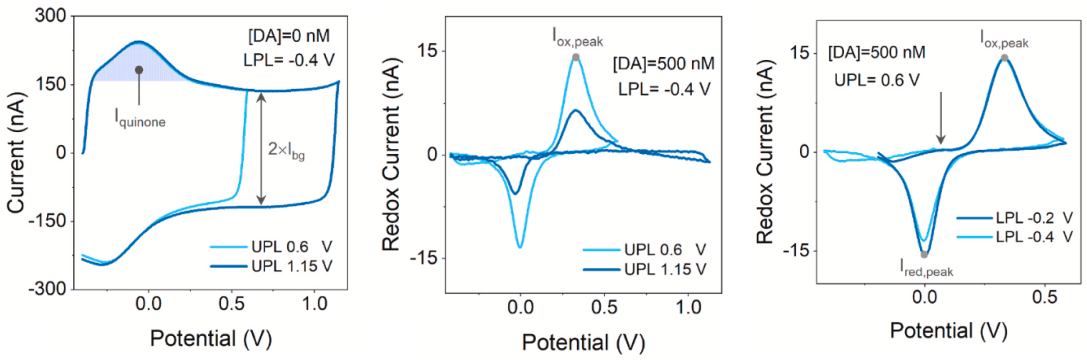

Figure 3.6: UPL and LPL variation effects on the triangular waveform [9]

The same study was performed with the LPL. In this case, only negligible effects were visible when switching to less negative potential values (3.6). No other key features of the voltammogram showed visible changes, but it is important to note that this type of behavior of the NG sensor is in contrast to other carbon sensors [48].
One of the main problems in trying to improve the sensitivity with the triangular waveform are some sources of interference. These include the current fluctuations generated by quinone-like species. These current variations become important when the local pH level changes significantly [49, 50]. Eliminating this interference was essential to achieve lower detection limits.
The solution was to develop an N-shaped waveform (3.7). This new type of waveform produced similar results in terms of UPL and LPL effects, but it was essential to reduce the magnitude of the current associated with quinone-like species in both the background (3.7) and cyclic voltammogram (3.7) recordings. This waveform engineering was a direct consequence of the disparate voltage dependence characteristics of the NG micro-sensors.

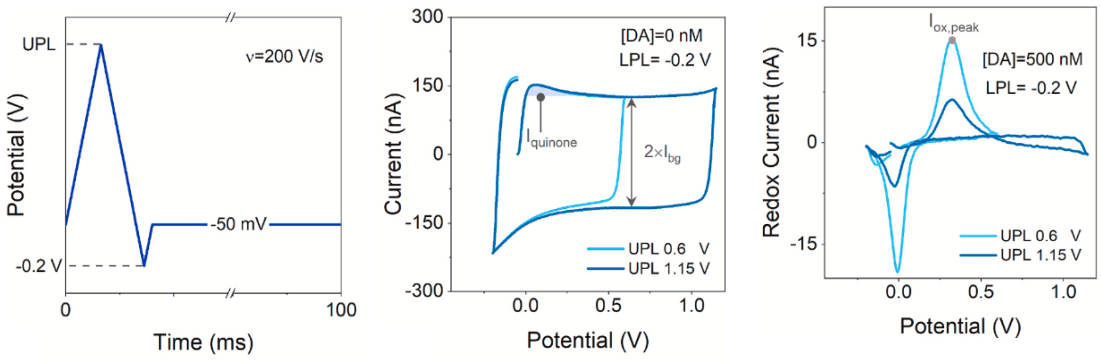

Figure 3.7: N-shaped waveform with background and cyclic voltammogram [9]

The sensitivity dependence of the NG sensor on the UPL could be attributed to a change in the number of adsorbed DA molecules. DA is positively charged at the physiological pH due to the protonation of the amine side chain [51, 52] so the electrostatic force induced by the positive UPL is critical to establish the number of adsorbed molecules.

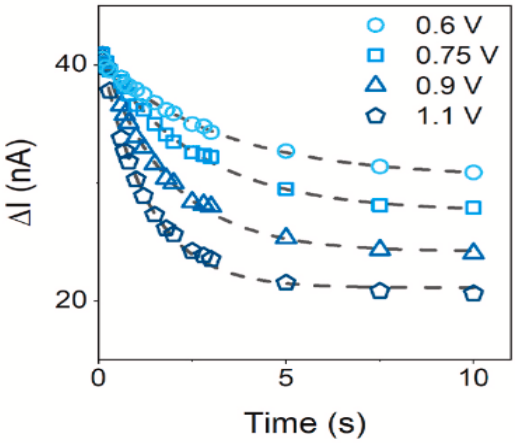

Figure 3.8: Time evolution of the ox peak height for different UPL with $1\mu M$ DA [9]

The number of adsorbed molecules decreases with time until equilibrium is reached; the initial value is almost the same for all measurements; finally, a larger UPL causes a larger repulsive force, which pushes away more molecules with each cycle until equilibrium is reached (3.8) [9].

Serotonin detection

Serotonin (5HT), like DA, is a neurotransmitter found in the brain and plays a role in psychiatric and neurological disorders. The problem with FSCV measurement of 5HT is that the carbon sensors become fouled in the process and this phenomenon is due to the presence of side reactions that generate byproducts [53, 54, 55, 56]. The cyclic voltammogram obtained with the conventional waveform is characterised by the presence of a shoulder adjacent to the primary oxidation peak, which is due to these side reactions (3.9) [57].

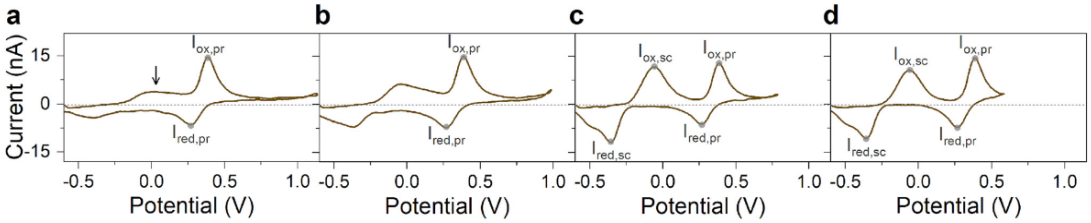

Figure 3.9: Serotonin cyclic voltammogram with a traditional waveform and UPL of 1.15V, 1.0V, 0.8V and 0.6V [57]

More specifically, the secondary peak could be associated with the redox reactions of tryptamine 4,5-dione, as its standard potential was estimated to be -0.21V. This particular compound is formed by a chemical reaction involving water (3.10 III) and it was also observed that the secondary peak increased up to a UPL of 0.8V and then decreased.

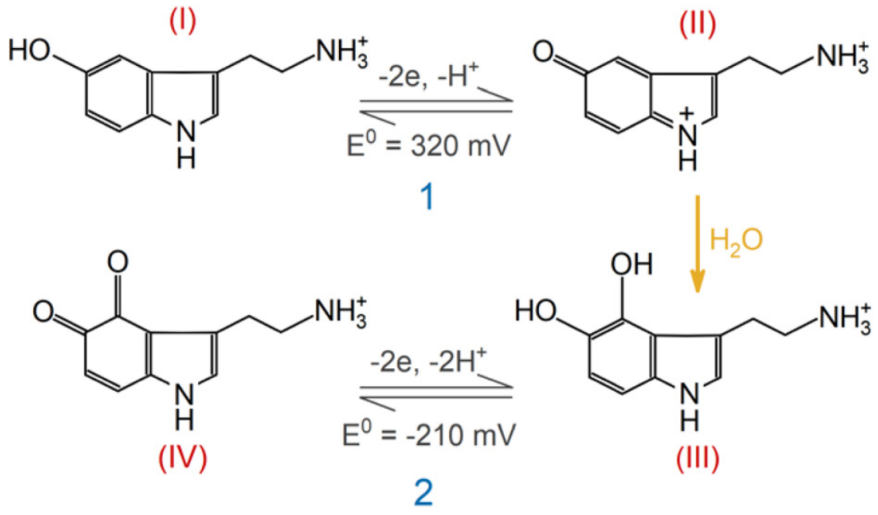

Figure 3.10: Serotonin primary and secondary redox reactions [57]

This specific value corresponds to the onset of water oxidation at pH 7.4; this water reaction is the cause of the formation of chemically active species that deplete the intermediate compound and cause the secondary peak in the cyclic voltammogram to turn into a broad shoulder peak (3.9). The strategy to obtain better results was to develop a waveform with a potential sweep rate that avoids the water oxidation reaction [57].
Also in this case, an N-shaped waveform was developed. Since the onset of water oxidation is at 0.8V, measurements were made with a UPL below this value, also taking into account that at least 0.6V are necessary to capture the entire 5HT primary oxidation peak at a scan rate of 200V$s-1$. At the same time, the standard potential of the secondary reaction byproduct is -0.21V, setting the minimum for the LPL at 0.2V [57]. Based on the same reasoning, it was also found that oxidation of this compound is greatly reduced with a holding potential of at least -0.1V, while sensitivity to 5HT remains constant at values below 0.2V (3.11).

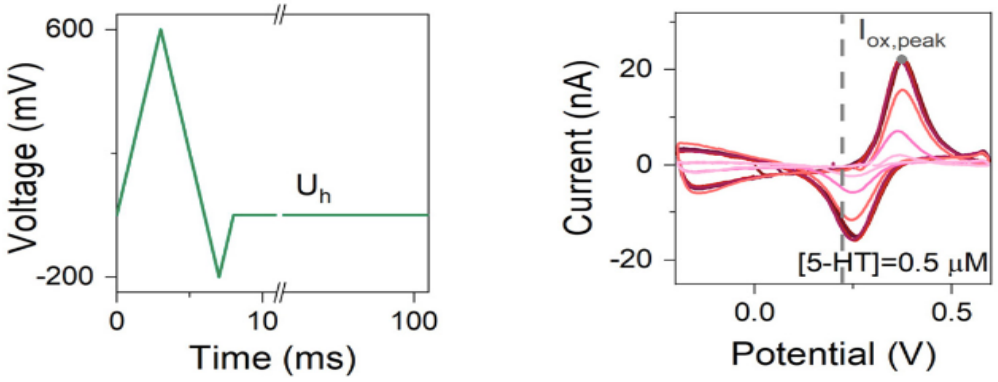

Figure 3.11: Example of engineered waveform and voltammogram for serotonin detection [57]

The combination of the NG sensor and the constructed waveform resulted in a detection limit of about 5nM, which is below physiological levels in the brain [57]. Moreover, an additional result was an improvement in the sensor's resistance to fouling. This phenomenon usually manifests itself already after the first few trials [56], but during the study with the new waveform the sensitivity was almost unchanged even after fifteen trials.

Melatonin detection

Melatonin (MT) is another important hormone associated with important roles such as circadian rhythm regulation and has anti-inflammatory properties for the immune system. There are few methods to measure MT changes in real time

with high specificity and the ability to do so during inflammation could provide important information about the immunomodulation.
MT is an electroactive indoleamine that is easily oxidised at carbon electrodes. The products formed by this oxidation electopolimerise in solution, which can lead to strong adsorption and to sensor fouling [58]. To maintain the low detection limit while avoiding electrode fouling, a special waveform is required.

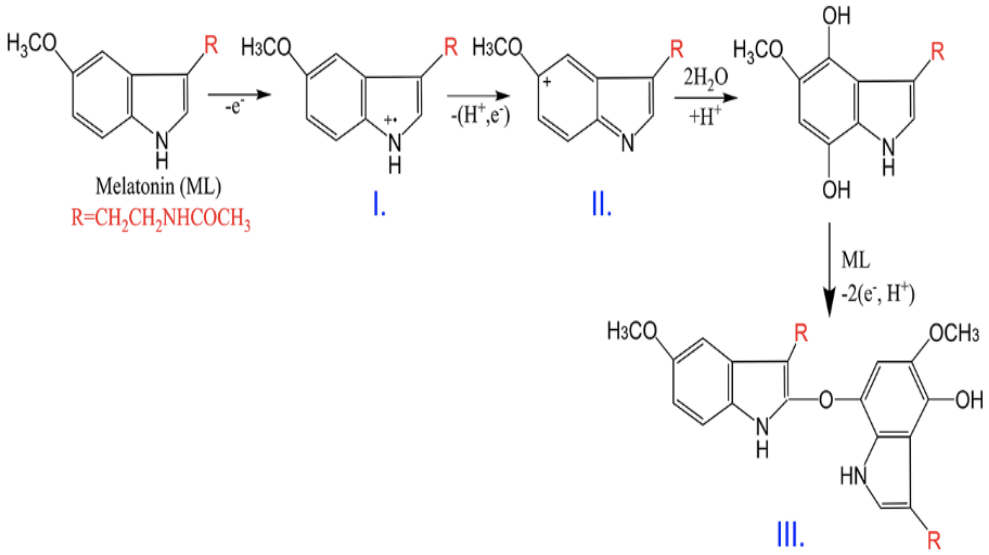

Figure 3.12: Melatonin oxidation reactions [59]

The first reaction of MT during the measurements is the loss of an electron (3.11 I), followed by another oxidation process consisting of the loss of an electron and a proton, leading to the formation of a highly reactive quinonimine (3.11 II). This causes electropolymerisation in the solution and can lead to contamination of the sensor by adsorption of unwanted products [58].
Several studies with carbon-fiber micro electrodes showed the presence of three distinct peaks when using the traditional waveform: the primary one at 1.0V (3.11 I), a small secondary one at 1.1V during the back scan (3.11 II) and a third one at 0.6V caused by electropolymerisation in solution (3.11 III). The position of these peaks was determined by the value of the scan rate, with a higher value that could shift them at higher potentials [58].
Various parameters were varied to minimise fouling of the sensor. Increasing the UPL resulted in an increase in both the primary peak and the tertiary fouling peak (3.11 A). On the other hand, increasing the holding potential resulted in a greater decrease in the oxidation peak associated with fouling than in the primary one: the fouling peak became negligible at a holding potential of 0.2V, which was then chose as the LPL (3.11 B).

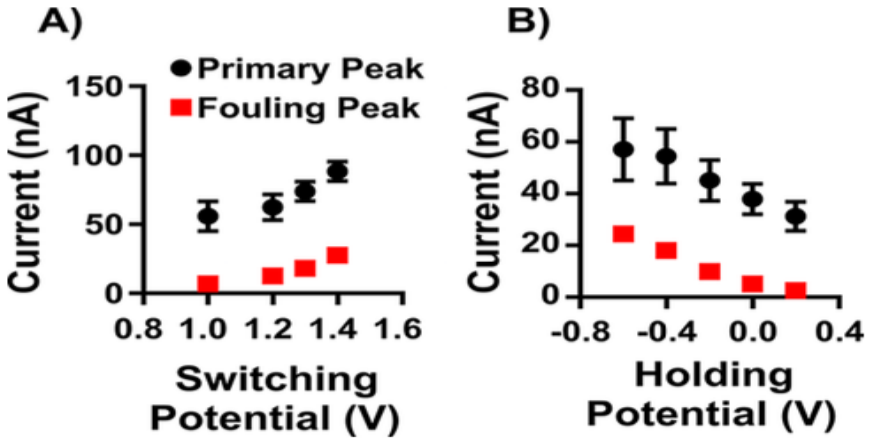

Figure 3.13: UPL and LPL effects of the sensitivity [59]

A final consideration is that MT's oxidation process on carbon-based surfaces is diffusion controlled and for this reason it was confirmed that a frequency of 10Hz was the optimal choice [58]. The final waveform developed for MT provided a reduction in fouling, resulting in a much more stable detection over time and a smaller detection limit [59].

3.2 Electrochemical Impedance Spectroscopy

Electrochemical Impedance Spectroscopy (EIS) is largely used in chemical sensing and biosensing as it provides kinetic and mechanistic data of various electrochemical systems. A system in an equilibrium condition is perturbed by applying a sinusoidal signal over a large range of frequencies and the response is observed. EIS works as a "transfer function" that models the output signal to the input one; this is because there is a linear relation between the two and the system behaviour is time invariant. EIS is able to provide information for various kind of processes that exhibits highly different time behaviours [60].
This technique consists in the simulation of an electrochemical system as an equivalent electrical circuit, composed just by passive and distributed components, different for every type of simulated process. EIS can deconvolute a complex system in a combination of individual processes that can be easily analysed when working in the frequency domain instead of the time one. The frequency range is limited by the available technology, but it usually goes from 10μHz to 1MHz. In practice the actual frequency range is selected in an experimental logic [60].
For the measurements the perturbation must be of a small amplitude in order to obtain an almost linear response, because in a real system, as the one analysed

during this project, the current-voltage relationship is not actually linear. The validity of the data can be evaluated by using the Kramers-Kronig relations, which are used to find the impedance real part starting from the imaginary one and vice versa. This dependence between the two is fundamental and it depends on four factors: the system must be linear, i.e. input and output signals must involve the same frequency; the response must be completely input-dependent; the system must come back to its original state after the perturbation is ended and the real and imaginary part must be of finite values over the all frequency range. This last parameter can be checked only by introducing some approximations.
The obtained data can then be analysed and plotted in different formats; the two most common ones are the Bode plot and the Nyquist plot. For the latter one the imaginary part of the impedance is plotted against the real part of it at each excitation frequency. This type of representation has two shortcomings: there is a lack of direct frequency-impedance matching and there is a non-distinct display of the spectrum in the high frequency range. On the other hand, there are two different Bode plot, one where $-phase = f(log(f))$ and one where $log(|Z|) = f(log(f))$. In these case there is a matching between the excitation frequency and the phase or the module of the impedance, with the addition that, being in logarithmic scale, a broad frequency range of data is clear (3.14) [60].

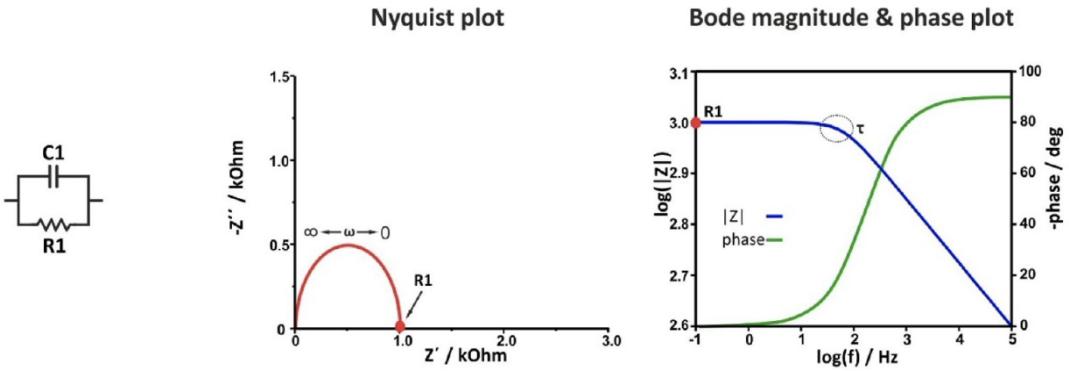

Figure 3.14: Nyquist and Bode plots examples [60]

Chapter 4

Results

The goal of the project was to determine how the different ion concentrations of the buffer solution would have affected the sensitivity of the sensor. Several experiments were conducted using different sensors. In these measurements, two parameters were varied: the concentration of the buffer solution and the type of bioanalyte.

4.1 Calibration curve

Prior to the actual measurement of the effects of the ion concentration, a calibration step was performed to observe the dependence of the redox current on the bioanalyte concentration.

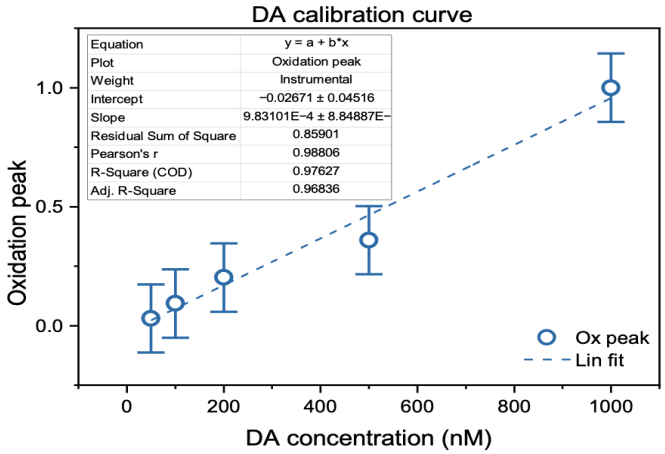

Figure 4.1: Calibration curve associated to the DA voltammogram

The first step of the experiment was a conditioning operation. This consisted of

injecting 1X PBS (at a rate between 0.2mL/min and 2mL/min) into the chamber while monitoring the response of the sensor, i.e. the background current. During this process, the background varies in its dimensions until the final, almost stable shape is reached. When this process is performed for the first time with a new sensor, it takes different lengths of time. When using a sensor already conditioned in a previous experiment instead, this part will take about 20/30 minutes.
For the actual experiment, the flows of PBS and the analyte were used alternately: first PBS was injected at 30mL/min for 15 seconds, then the flow was switched to the analyte at 30mL/min for 20 seconds, and finally it was switched back to PBS to clean the sensor after detection. The same procedure was repeated for different concentrations of the bioanalyte. The final result showed the linearity of the sensor over a wide range of concentrations (4.1).

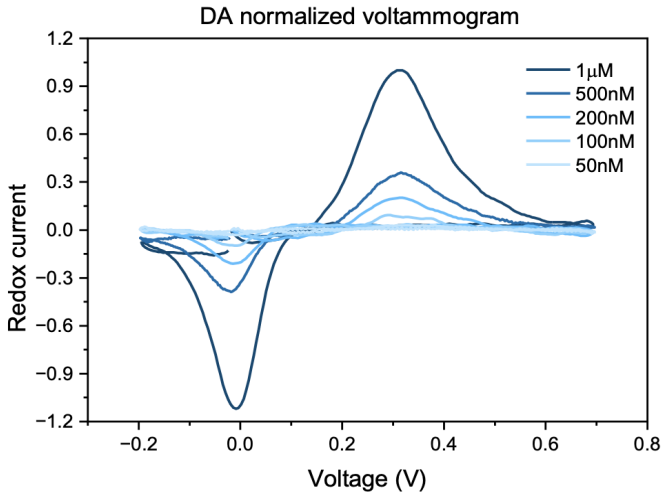

Figure 4.2: Example of cyclic voltammogram for DA

Furthermore, several observations can be done by looking at the voltammogram (4.2). Its shape is characteristic of each detected molecule, with some specific parameters that can be used to identify the detected bioanalyte, i.e. they can be considered as its fingerprint. In the example of figure (4.2) it is possible to see how the two peaks are symmetrical and go back to zero. Another feature is that the peak current for the oxidation of DA is larger than that for the reduction of DoQ, with a ratio between them $I_{ratio} \approx 0.8$. In addition, the position of the actual oxidation peak ($\approx 0.32V$) and the distance between the two ($\Delta E_p \approx 0.33V$) are also determined by the type of the target analyte and of the waveform. The smaller the ratio between the two peaks and the larger ΔE_p are, the slower the electron transfer and the worse the sensor works [46, 61]. Finally, a last important parameter is the amplitude of the oxidation peak. The larger the value, the more sensitive the sensor is. A good way to measure this value is the SBR, which is

calculated for a concentration of 1µM as follows:

$$SBR = \frac{2I_{Ox}}{I_{OxBack} + I_{ReBack} - I_{par}} \tag{4.1}$$

Where I_{Ox} is defined as the amplitude of the oxidation peak, I_{OxBack} and I_{ReBack} as the amplitudes of the oxidation and reduction background currents, and I_{par} as the parasitic current. In the presented work, the aim was not to have a sensor with the best possible sensitivity, so an SBR of ≈0.2, was considered acceptable. The difference in height of the two peaks is particularly important. In a reversible reaction there would be no difference, so it is a non-reversible reaction [46]. This is due to the difference in adsorption of DA and DoQ. DA adsorbs much more strongly on carbon electrodes than DoQ, in other words DoQ is more likely to be desorbed from the surface before being reduced back to DA [62].
The results of this first set of experiments are summarised in the following table (4.1).

I_{ratio}	Ox peak FWHM (V)	Ox peak position (V)	ΔE_p	SBR
0.8	0.17	0.32	0.33	0.20

Table 4.1: DA calibration curve results

4.2 EIS measurements

In addition to the FSCV measurement, an EIS study was also carried out with several sensors.

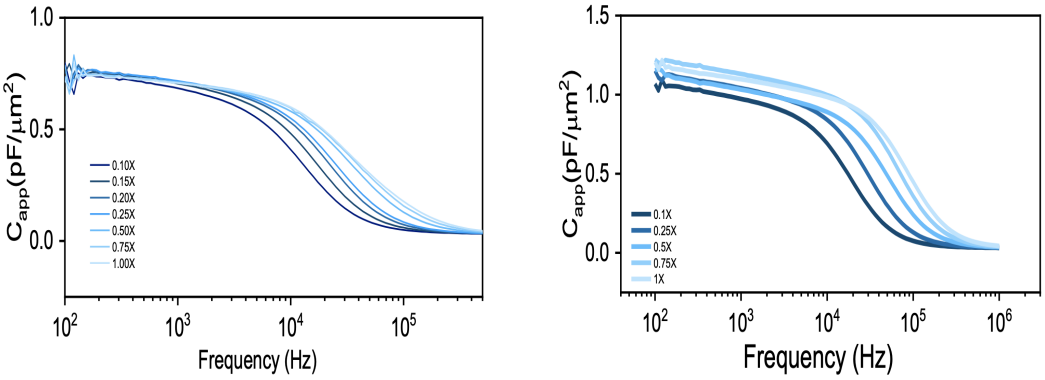

Figure 4.3: Example of a sensor Bode plots (module)

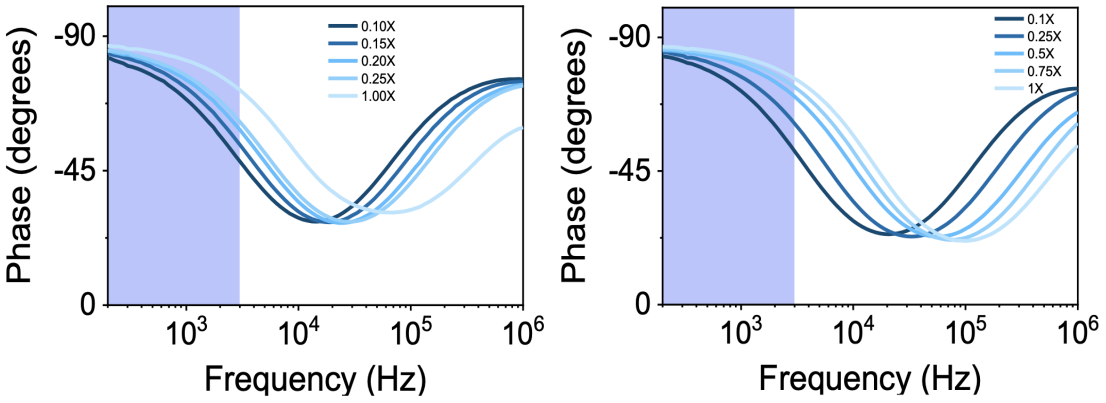

Figure 4.4: Example of a sensor Bode plots (phase)

Based on the Bode plots, it could be confirmed that the structural properties of the NG sensors gave them an almost capacitive behaviour. In particular, for the frequencies of interest in the FSCV measurements, i.e. below 3kHz, the frequency response plot showed a slight decrease of less than 10% (4.3), while the phase response for 1X PBS was around -90° and became slightly smaller at lower concentrations (4.4). These results demonstrated that the sensors were maintaining their desired behaviour in the range of interest, but deteriorated at lower concentrations of ions in the buffer solution. Compared to conventional carbon sensors, which have a mixture of resistive and capacitive behaviour, the difference typical of these NG sensors is still visible [63, 64].

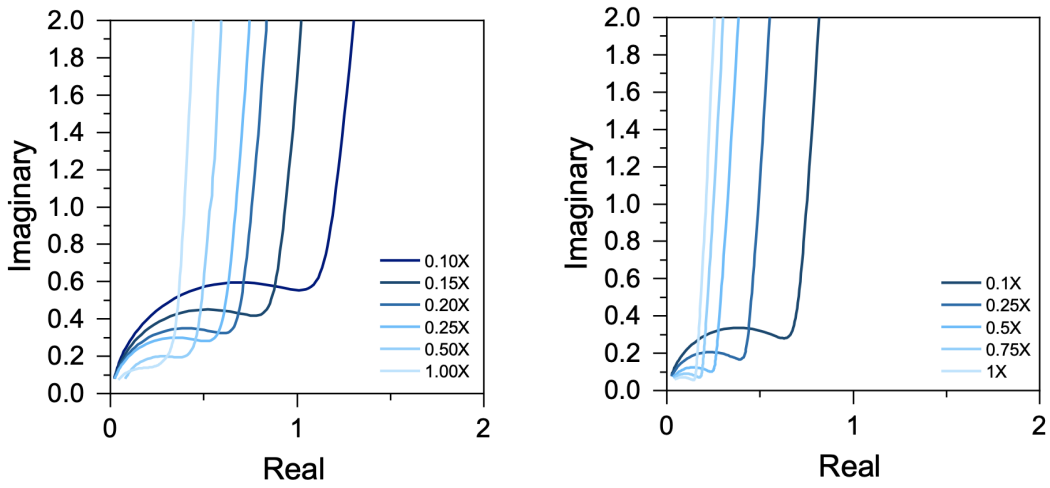

Figure 4.5: Example of Nyquist plots

After the Bode diagrams, the Nyquist ones were also useful to obtain important information. Their patterns involve a semicircle and then a straight line; these two behaviours represent the two frequency ranges in which the electrochemical process is determined by the charge transfer phenomena and the mass transfer one, respectively. For a reaction to be reversible, the charge-transfer resistance (R_{ct}), i.e. the diameter of the semicircle, becomes insignificantly small and the so-called Warburg impedance (Z_W) is dominant over almost the entire frequency range. In this case, the semicircle is not well defined because the mass transfer phenomena is predominant. The reported Nyquist diagrams confirm what was also seen in the Bode diagrams. The sensors are characterised by an almost capacitive behaviour, which approaches a mixed resistive-capacitive behaviour with decreasing concentration of ions in the buffer solution (4.5).

4.3 Bioanalytes analysis

4.3.1 Background recordings

Prior to measuring the analyte response when the buffer ion concentration was varied, the background current was recorded using the conventional waveform (from -0.4V to 1.3V or 1.2V with a repetition rate of 60Hz and a ramp rate of either 400V/s or 200V/2). Interestingly, the shape of the background current varied with the buffer ion concentration (4.6).

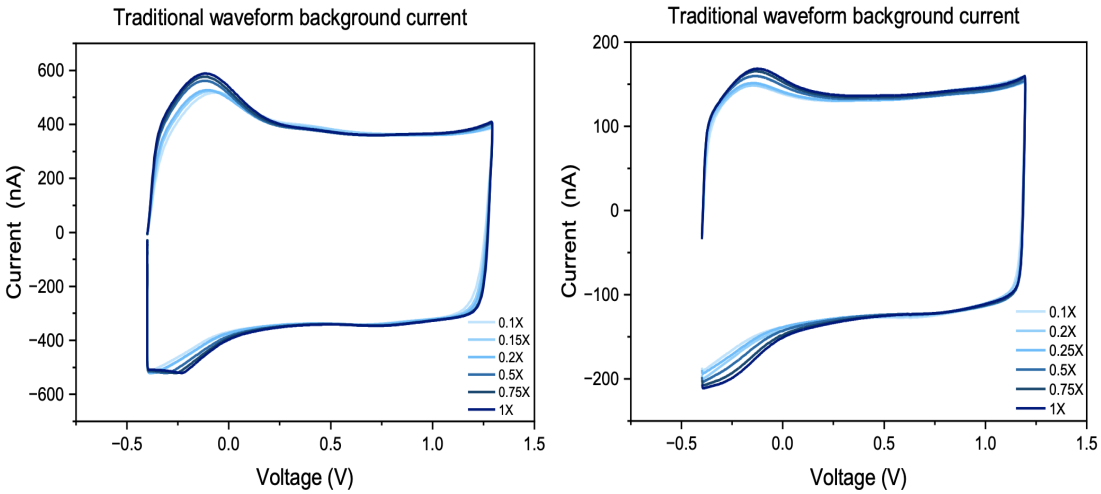

Figure 4.6: Background current recordings for different sensors

As expected, a similar behaviour was obtained for both the recorded cases. The first

parameter change observed was the difference between the peak of the background current and the point at which it flattens out (ΔI_{bg}), i.e. the voltage at which the capacitive behaviour of the sensor becomes apparent. While the second point was fixed at all buffer concentrations ($\approx 0.6V$) and had an almost constant value, the position and value of the peak seemed to depend on the concentration in different ways. (4.7).

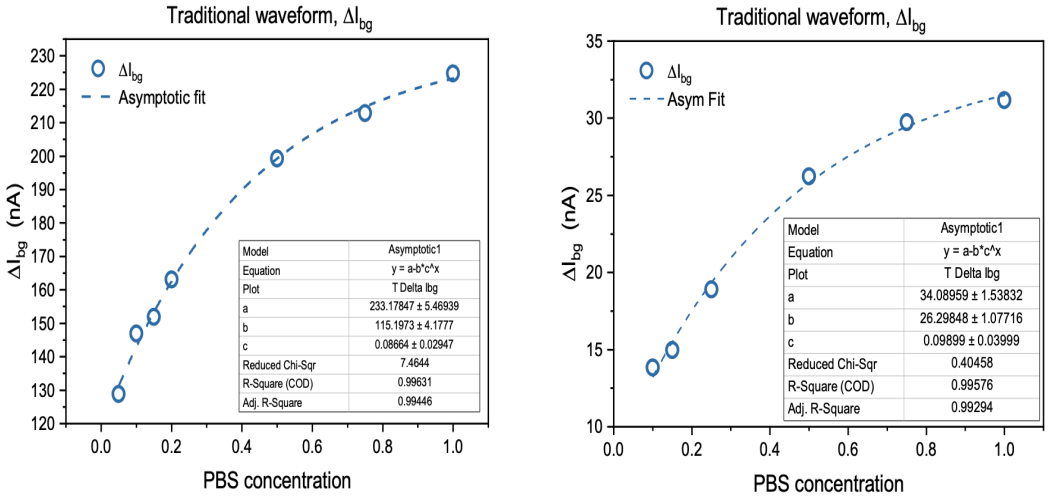

Figure 4.7: ΔI_{bg} measured for the different backgrounds

The relevant parameters extracted from the obtained results are also listed in tables (4.2) and (4.3).

PBS concentration	Current peak value (nA)	ΔI_{bg} (nA)
0.10X	517.66	146.90
0.15X	523.59	154.90
0.20X	526.61	165.06
0.50X	561.37	199.27
0.75X	576.39	212.82
1.00X	588.08	224.66

Table 4.2: Background recording results for a 400V/s ramp rate

PBS concentration	Current peak value (nA)	ΔI_{bg} (nA)
0.10X	148.50	13.83
0.15X	149.58	14.96
0.25X	151.39	18.90
0.50X	159.84	26.23
0.75X	165.45	29.73
1.00X	168.40	31.16

Table 4.3: Background recording results for a 200V/s ramp rate

4.3.2 Dopamine measurements

The first bioanalyte analysed was DA, a catecholamine. It is the simplest possible one, consisting of a catechol structure with one amine group attached via an ethyl chain. It is also a positively charged molecule.

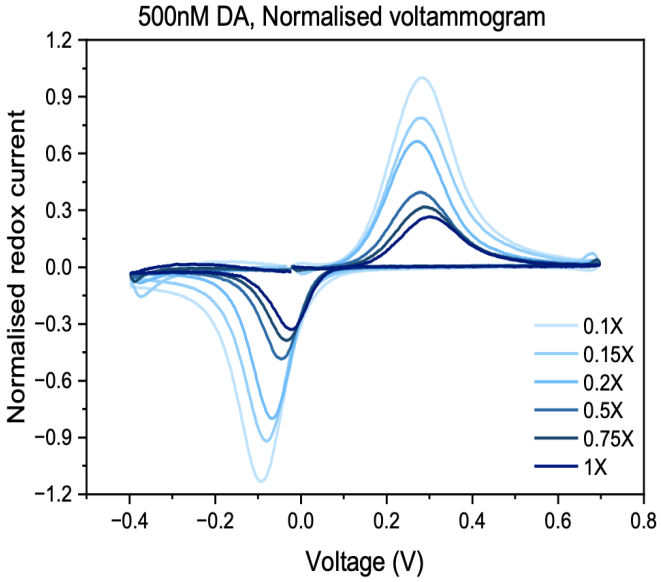

Figure 4.8: 500nM DA cyclic voltammogram for different PBS concentrations

A solution of 500nM DA was measured for all previous buffer concentrations (4.8) with the DA optimised waveform (from -0.4V to 0.7V with 400V/s ramp rate and 10Hz repetition rate). Several observations could be made. First, the sensitivity of the sensor increased with an exponential trend while the PBS concentration decreased (4.9).

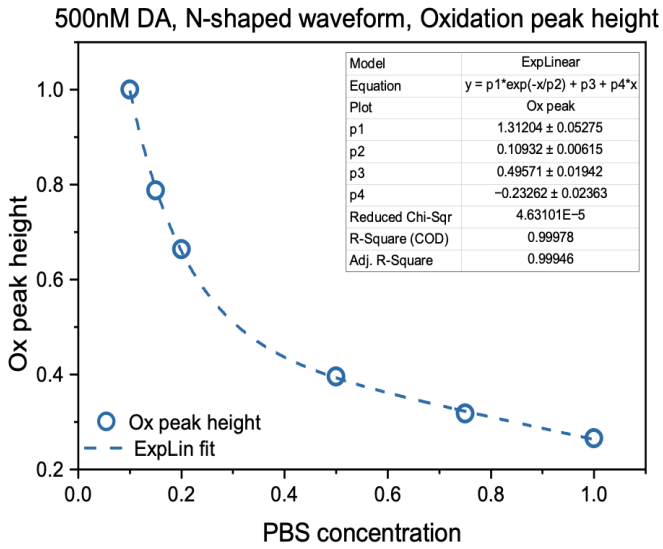

Figure 4.9: Oxidation peak height trend for DA

This exponential increase was also associated with a very similar increase in the measured SBR, indicating that the detection limit could be lowered (4.10).

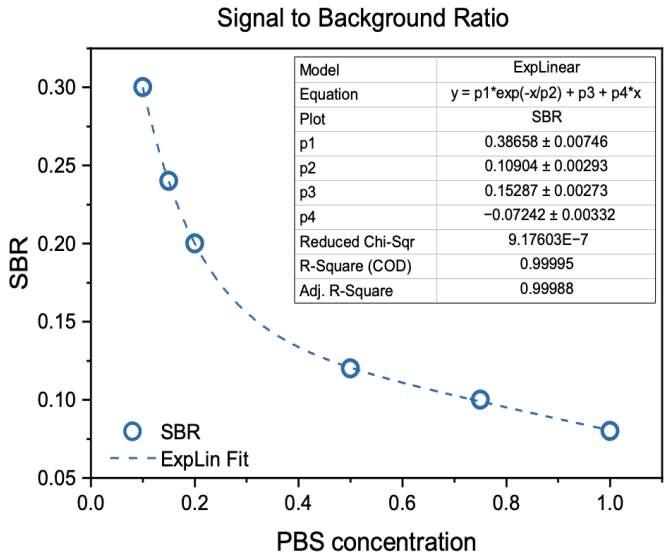

Figure 4.10: Signal to background ratio trend for DA

At the same time, the voltage gap between the oxidation and reduction peaks (ΔE_p) also followed a similar exponential trend, with the difference that it was more pronounced at the lower concentrations, while it was almost constant at the higher ones (4.11).

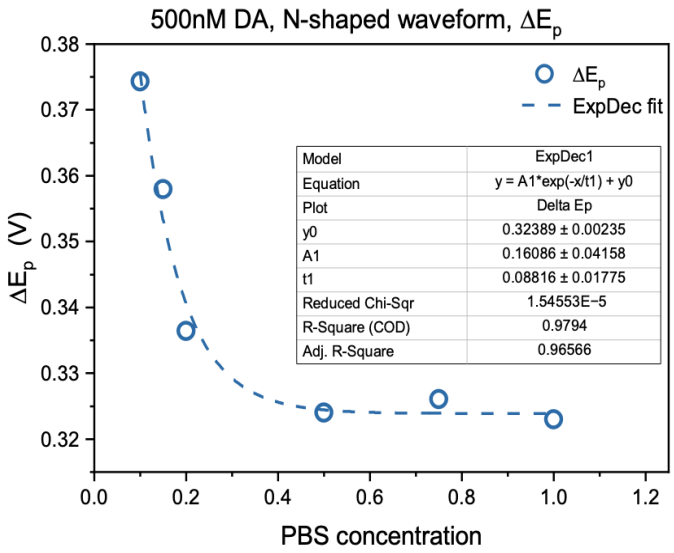

Figure 4.11: ΔE_p trend for DA

This change in values could be attributed to two different factors. A change in the ion concentration of the buffer solution caused both the oxidation and reduction peaks to shift to lower potentials. At the same time, the lowest concentrations of PBS also led to a shift of only the reduction peak to a higher potential, increasing the ΔE_p and resulting in a slower electron transfer kinetics (4.12).

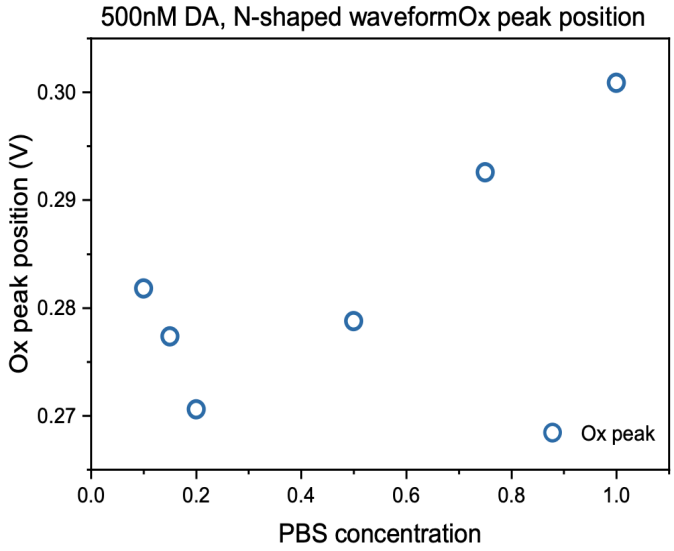

Figure 4.12: Oxidation peak position trend for DA

The slower electron transfer kinetics was also confirmed by looking at the rise

time, which was nearly constant for the higher buffer concentrations and increased linearly with decreasing ion in solution (4.13). At the same time, there were no changes in the area ratio between the two peaks or in the shape of the peaks (the FWHM remained constant in all measurements).

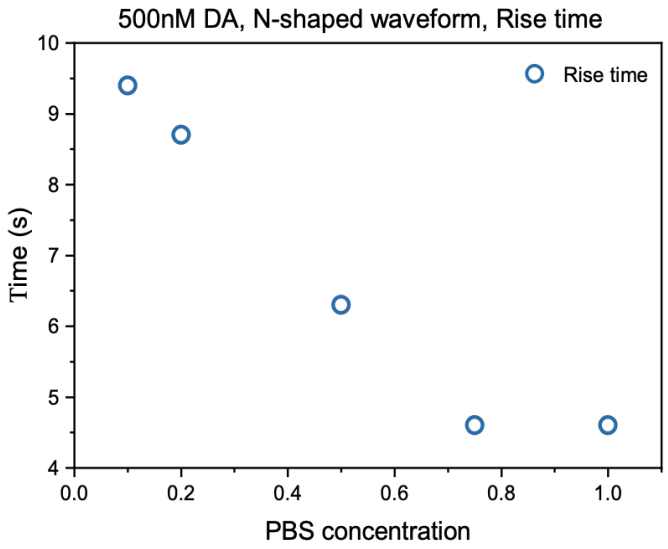

Figure 4.13: Rise time trend for DA

The relevant parameters extracted from the obtained results are also shown in table (4.4).

PBS concentration	0.10X	0.15X	0.20X	0.50X	0.75X	1.00X
Ox peak height	1.0000	0.7878	0.6639	0.3952	0.3175	0.2658
SBR	0.30	0.24	0.20	0.12	0.10	0.08
ΔE_p (V)	0.3743	0.3579	0.3364	0.3240	0.3261	0.3230
Ox peak position (V)	0.2818	0.2774	0.2706	0.2788	0.2926	0.3009
Rise time (s)	9.4	/	8.7	6.3	4.6	4.6
FWHM (V)	0.17	0.17	0.17	0.17	0.17	0.17
I_{ratio}	0.8118	0.8000	0.8148	0.8125	0.8077	0.8182

Table 4.4: DA measurement results

4.3.3 Melatonin measurements

A second set of measurements was performed with a different type of bioanalyte, MT, which is neither a catecholamine nor a charged molecule.

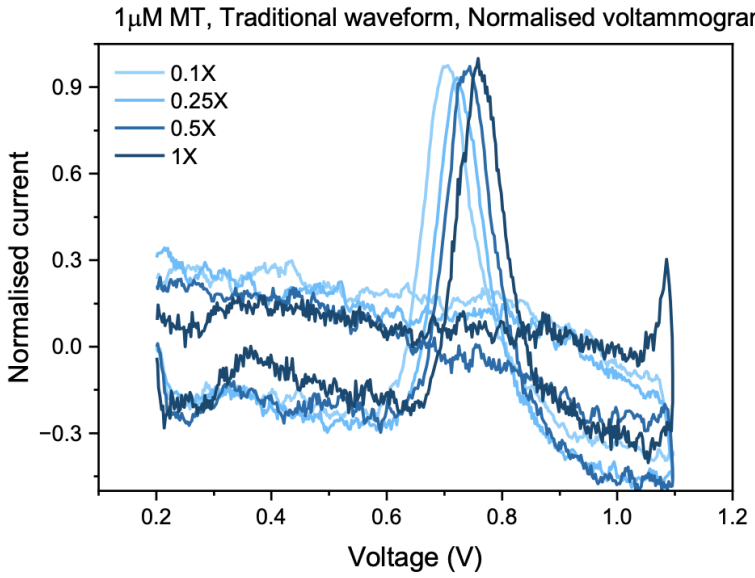

Figure 4.14: $1\mu M$ MT cyclic voltammogram for different PBS concentrations

The optimised waveform MT was used to measure the analyte (from 0.2V to 1.1V with 200V/s of ramp rate and a repetition rate of 10Hz).

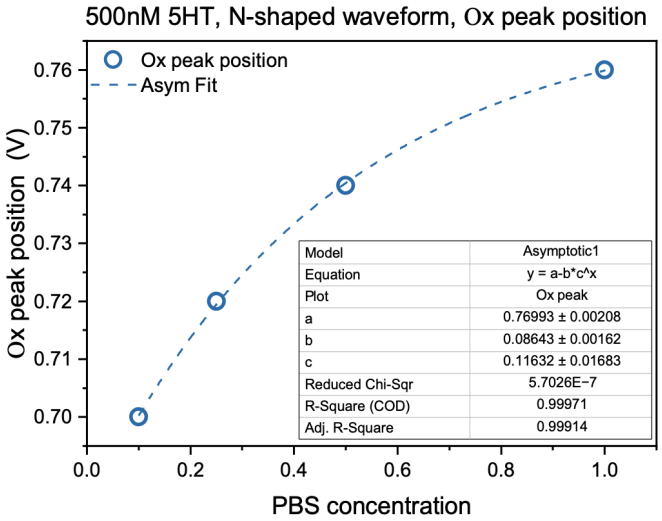

Figure 4.15: Oxidation peak position trend for MT

The cyclic voltammogram showed a different behaviour than in the DA case. The sensitivity of the sensor was completely unchanged, while the ion concentration of the buffer solution varied (4.14).
Moreover, the characteristic quantities, which were also analysed during the DA experiments, remained unchanged for all different concentrations. The only observable difference was the same shift of the oxidation peak to lower voltages when the ion buffer concentration was decreased (4.15).
The extracted numerical results are also shown in table (4.5).

PBS concentration	Ox peak position (V)	Ox peak height
0.10X	0.70	0.9727
0.25X	0.72	0.9328
0.50X	0.74	0.9719
1.00X	0.76	1.0000

Table 4.5: MT measurement results

4.3.4 Serotonin measurements

Finally, another type of bioanalyte was examined. In this case, the 5HT molecule was observed, which is a charged molecule like DA but not a catecholamine, like MT.

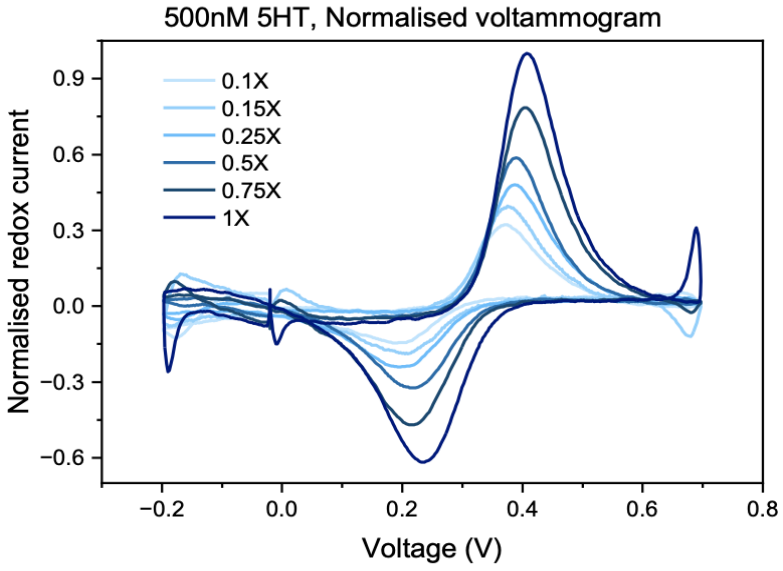

Figure 4.16: 500nM 5HT cyclic voltammogram for different PBS concentrations

Also in this case, a solution of 500nM was injected at the same buffer concentrations and measured with the optimised 5HT waveform (from -0.2V to 0.7V with 200V/s of ramp rate and 10Hz of repetition rate) (4.16). A different behaviour was observed for this type of molecule than for the other two categories.

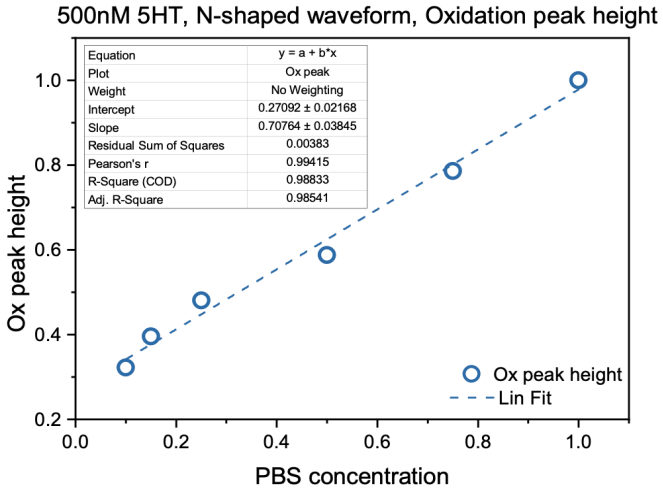

Figure 4.17: Oxidation peak height trend for 5HT

The sensitivity of the sensor showed a linear decrease with decreasing buffer ion concentration (4.17).

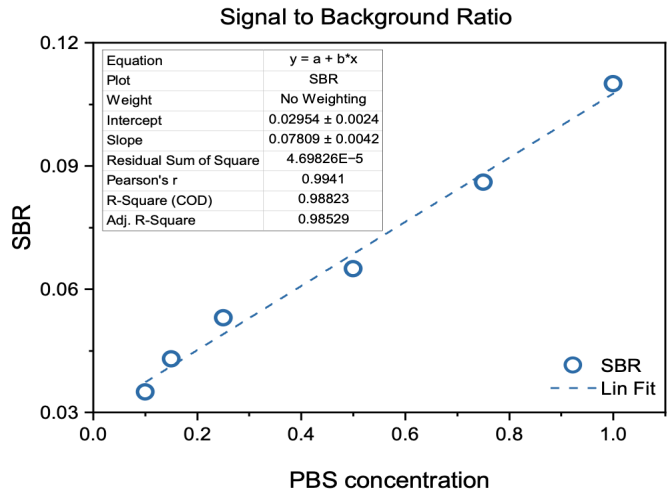

Figure 4.18: Signal to background ratio trend for 5HT

As expected, this linear decrease was also associated with a comparable behaviour of the SBR (4.18).

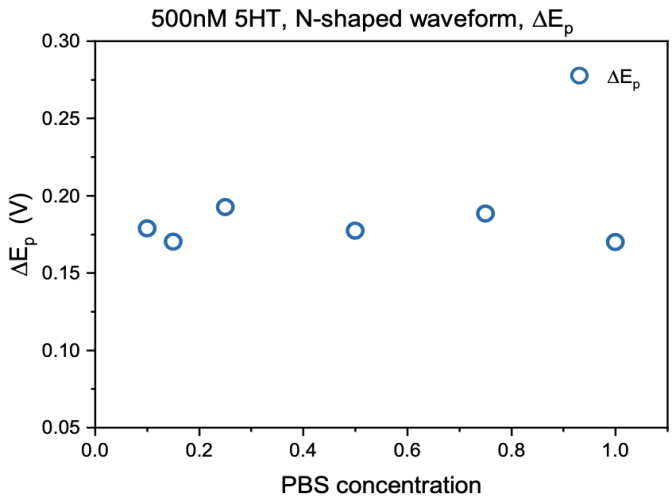

Figure 4.19: ΔE_p trend for 5HT

Unlike DA, the ΔE_p remained nearly constant for each measurement and showed no dependence on the buffer ion concentration in the solution (4.19).

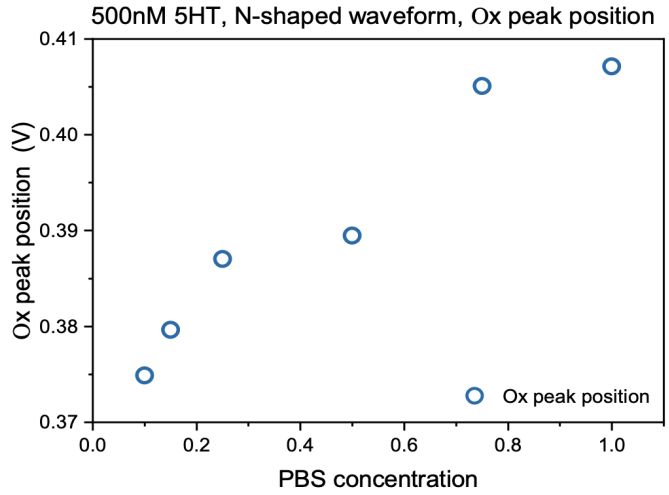

Figure 4.20: Oxidation peak position trend for 5HT

Looking at the position of the oxidation peak (4.20), a similar type of decrease was observed, which means that the reduction peak also followed the same trend to show a nearly constant ΔE_p.

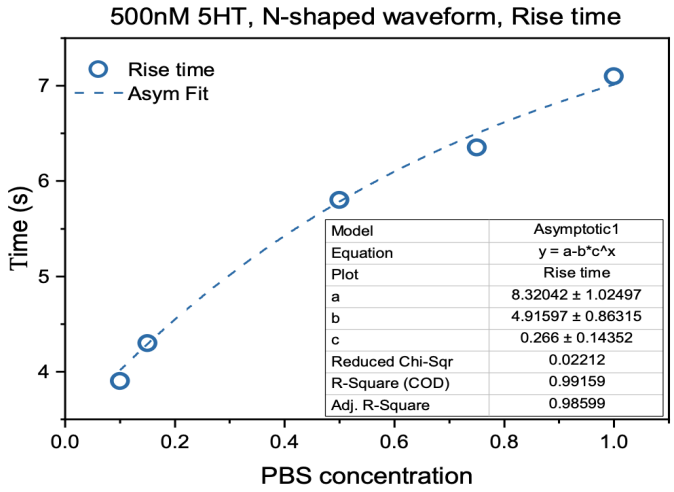

Figure 4.21: Rise time trend for 5HT

Finally, the rise time showed a non-linear behaviour, with a faster response for the lower buffer ion concentrations.
The same constant behaviour was also observed in this case for both the ratio between the peak areas and their shape.
The relevant parameters extracted from the results obtained are also shown in table (4.6).

PBS concentration	0.10X	0.15X	0.25X	0.50X	0.75X	1.00X
Ox peak height	0.3224	0.3928	0.4802	0.5878	0.7858	1.0000
SBR	0.035	0.044	0.053	0.066	0.085	0.110
ΔE_p (V)	0.1787	0.1703	0.1925	0.1774	0.1885	0.1700
Ox peak position (V)	0.3749	0.3796	0.3870	0.3895	0.4051	0.4071
Rise time (s)	3.9	4.3	/	5.8	6.35	7.1
FWHM (V)	0.13	0.13	0.13	0.12	0.12	0.12
I_{ratio}	0.8182	0.8333	0.8000	0.7778	0.8077	0.8235

Table 4.6: 5HT measurement results

4.3.5 Results discussion

Some considerations can be made. First of all, the only part of the background current that was significantly affected was the peak associated with the quinone-like species, i.e. the peak of the background current just before the 0V potential. A

first hypothesis is that this change is due to a change in the pH of the buffer solution. It has already been mentioned that these current fluctuations attributed to quinone-like species are highly dependent on pH changes. It was confirmed that different ion concentrations in the buffer solution resulted in a different final pH value and thus a different current value (4.22).

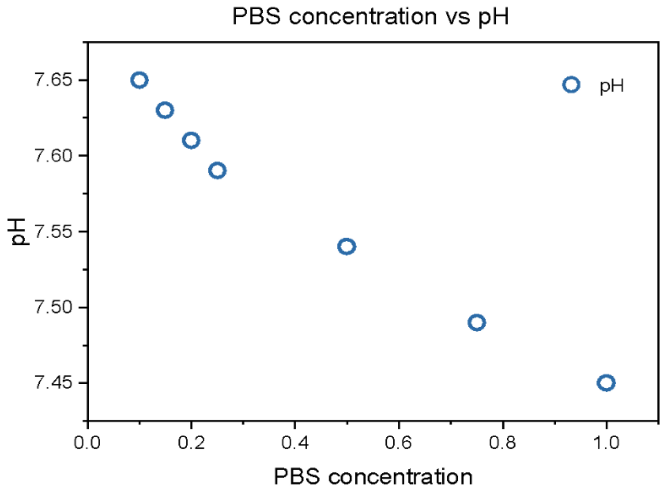

Figure 4.22: pH values of the buffer solution with different PBS concentration

Furthermore, when looking at the voltammogram, there is an effect that is similar for all three types of molecules studied: a decrease in the ion buffer concentration results in a shift of the oxidation peak in the voltammogram to lower voltages. The hypothesis was that this shift is due to a change in the reference potential of the Ag/AgCl electrode used as a gate. This value depends on a voltage jump between the metal of the wire and the buffer solution; a change in the ion concentration modifies this voltage jump and thus the value of the reference potential. Unfortunately, in the case of the catecholamines, there was also an increase in the voltage spread between the oxidation and reduction peaks that is opposite to this phenomenon and when comparing the other two types of molecules, the shift was more pronounced in one case. For this reason, it is possible that more factors are involved in this shift.
Furthermore, when looking at the different types of molecules, it was also observed how differently they react when the ion concentration in the buffer solution is varied. Neutral molecules (such as MT) were not affected by this in any way. At the same time, charged molecules reacted in different ways depending on whether they were catecholamines (such as DA) or not (such as 5HT). For this reason, the chemical composition of the different bioanalytes must be studied in more detail in order to better understand the reasons for the different response to the ions in the solution during the sensing measurements.

Chapter 5

Conclusions

The experimental work started with the use of already optimized sensors, made with the necessary knowledge to have optimal characteristics and thus good sensitivity to the presence of bioanalytes in solution. The main objective of the project was to observe the behaviour of these sensors while changing the concentrations of buffer solution and bioanalytes. The FSCV method was used with optimised waveforms that increased the sensitivity and reduced the noise caused by side reactions.
The first part of the project focused on testing the linearity of the sensor when the neurotransmitter concentration was increased or decreased. As expected, the sensors reacted completely linear in the tested concentration range, i.e. in a range that is also possible in the human brain.
In the second part of the work, the buffer ion concentration was changed and the reaction to this change was observed.
Initially, the sensor response to the applied sinusoidal signal confirmed the desired capacitive behaviour for the standard buffer concentration. At the same time, as the ion concentration in the solution decreased, the sensors began to show a mixed resistive-capacitive behaviour, which is further from the optimal response, but still compares well to the fully mixed resistive-capacitive behaviour typical of the common carbon-based sensors.
Subsequently, the different bioanalytes were diffused on the sensor surfaces and their responses to the change in buffer ion concentration led to the conclusion that the chemical composition of the molecules under consideration was crucial for the sensitivity of the sensors to their presence. It was observed that the change in ion concentration affected the reference electrode, resulting in a shift to lower voltages of the oxidation and reduction peaks in the voltammograms for lower ion concentrations. This variation was different for the different types of bioanalytes, leading to the conclusion that the change in reference potential was not the only factor determining it. At the same time, dopamine, which is both a catecholamine and a charged molecule, showed an increased sensitivity to lower ion concentrations

and poorer electron transfer kinetic. Melatonin, which is neither a catecholamine nor a charged molecule, remained unaffected by the changes in buffer concentration. Finally, with serotonin, which is a charged molecule, the sensitivity decreased when decreasing the ion concentration in the buffer solution.
Further studies must be conducted to better understand the chemistry behind the different responses of the sensor to the different types of bioanalytes in order to optimise the detection process.

Appendix A

Chemicals

All chemicals were purchased from Sigma Aldrich.
The bioanalytes, like DA, were first dissolved in 1X PBS to form stock concentrations of 2mM. The 1X PBS (pH of ≈7.4) was obtained by dissolving, in 2 litres of deionised water, 16g of sodium chloride, 2.88g of sodium phosphate diabasic, 480mg of potassium phosphate monobasic and 400mg of potassium chloride.
The lower PBS concentrations were formed by diluting the 1X one in deionised water and were then used to dilute the stock solutions of bioanalytes to the desired concentrations.

Bibliography

[1] A. A. Grace. «The tonic/phasic model of dopamine system regulation: its relevance for understanding how stimulant abuse can alter basal ganglia function». In: *Drug Alcohol Dependence* 37.2 (1995), 111'–129 (cit. on p. 1).

[2] L. A. Sombers C. A Owesson-White M. F. Roitman, A. M. Belle, R. B. Keithley, J. L. Peele, R. M. Carelli, and R. M. Wightman. «Sources contributing to the average extra- cellular concentration of dopamine in the nucleus accumbens,» in: *J. Neuro- chemistry* 121.2 (2012), 252'–262 (cit. on p. 1).

[3] S. A. Siegelbaum Z. B. Rosen S. Cheung. «Mid brain dopamine neurons bidirectionally regulate CA3-CA1 synaptic drive With 32 × 32 Three-Electrode Voltammetry Pixels». In: *Nature Neuroscience* 18.12 (2015) (cit. on p. 1).

[4] E. Cuniberto A. Alharbi T. Wu, Z. Huang, K. Sardashti, K-D. You, K. Kisslinger, T. Taniguchi, K. Watanabe, R. Kiani, and D. Shahrjerdi. «Nano-engineering the material structure of preferentially oriented nano-graphitic carbon for making high-performance electrochemical micro-sensors». In: *Scientific Reports* 10.9444 (2020) (cit. on pp. 1, 4–8).

[5] L. R. Rathbun R. J. Wickham W. Solecki, N. M. Neugebauer, R. M. Wightman, and N. A. Addy. «Advances in studying phasic dopamine signaling in brain reward mechanisms». In: *Front Biosci (Elite edition)* 5 (2013), 982'–999 (cit. on p. 1).

[6] P. W. Glimcher A. S. Hart R. B. Rutledge and P. E. Phillips. «Phasic dopamine release in the rat nucleus accumbens symmetrically encodes a reward prediction error term». In: *Journal of Neuroscience* 34.3 (2014), pp. 698–704 (cit. on p. 1).

[7] K. L. Parent C. W. Atcherley K. M. Wood, P. Hashemi, and M. L. Heien. «The coaction of tonic and phasic dopamine dynamics». In: *Chemical Communications* 51.12 (2015), 2235'–2238 (cit. on p. 1).

[8] S. Pappata J. Delforge M. Bottlaender, C. Loch, and A. Syrota. «Absolute quantification by positron emission tomography of the endogenous ligand». In: *J. Cerebral Blood Flow Metabolism* 21.5 (2001), 613'–630 (cit. on p. 1).

[9] Z. Huang E. Cuniberto A. Alharbi, T. Wu, R. Kiani, and D. Shahrjerdi. «Anomalous sensitivity enhancement of nano-graphitic electrochemical microsensors with reducing the operating voltage». In: *Biosensors and Bioelectronics* 177.112966 (2021) (cit. on pp. 1, 15, 16).

[10] N. Wood A. Manickam K.-D. You, L. Pei, Y. Liu, R. Singh, N. Gamini, M. W. McDermott, D. Shahrjerdi, R. G. Kuimelis, and A. Hassibi. «A CMOS Electrochemical Biochip With 32 × 32 Three-Electrode Voltammetry Pixels». In: *IEEE J. Solid-State Circuits* 54.11 (2019), 298'–2990 (cit. on pp. 3, 11).

[11] Y. Zhang D. L. Bellin H. Sakhtah, A. Price-Whelan, L. E. Dietrich, and K. L. Shepard. «Electrochemical camera chip for simultaneous imaging of multiple metabolites in biofilms». In: *Nature Commun* 7.1 (2016), pp. 1–10 (cit. on p. 3).

[12] McCreery S. Ranganahtan R. L. «Electroanalytical performance of carbon films with near-atomic flatness». In: *Analytical chemistry* 73 (2020), pp. 893–900 (cit. on pp. 3, 4).

[13] R. Kiani T. Wu A. Alharbi and D. Shahrjerdi. «Quantitative principles for precise engineering pf sensitivity in graphene electrochemical sensors». In: *Advanced Materials* 31.1805752 (2019) (cit. on pp. 3, 5).

[14] S. M. Majji S. Ranganahtan R. L. McCreery and M. Madou. «Photoresist-derived carbon for microelectromechanical systems and electrochemical applications». In: *Journal of Electrochemical Society* 147.277 (2000) (cit. on p. 4).

[15] K. Kinoshita R. Kostecki X. Song. «Electrochemical analysis of carbon interdigitated microelectrodes». In: *Electrochemical and Solid State Letters* 2.465 (1999) (cit. on p. 4).

[16] D. Alliata R. Kostecki B. Schnyder, X. Song, K. Kinoshita, and R. Kotz. «Surface studies of carbon films from pyrolyzed photoresist». In: *Thin Solid Films* 396 (2001), pp. 36–43 (cit. on p. 4).

[17] R. J. Grigsby D.J. Fischer W. R. IV Vandaveer and S. M. Lunte. «Pyrolyzed Photoresist Carbon Electrodes for Microchip Electrophoresis with Dual-Electrode Amperometric Detection». In: *Electroanalysis: An International Journal Devoted to Fundamental and Practical Aspects of Electroanalysis* 17 (2005), pp. 1153–1159 (cit. on p. 4).

[18] A. J. Downard S. S. Yu. «Photochemical grafting and activation of organic layers on glassy carbon and pyrolyzed photoresist films». In: *Langmuir* 23 (2007), pp. 4662–4668 (cit. on p. 4).

[19] B. Moody M. K. Zacheck P. Takmakov, R. M. Wightman, and G. S. McCarty. «Simultaneous decoupled detection of dopamine and oxygen using pyrolyzed carbon microarrays and fast-scan cyclic voltammetry». In: *Analytical chemistry* 81 (2009), pp. 6258–6265 (cit. on pp. 4, 7).

[20] P. Takmakov M. K. Zacheck J. Park, R. M. Wightman, and G. S. McCarty. «Microfabricated FSCV-compatible microelectrode array for real-time monitoring of heterogeneous dopamine release». In: *Analyst* 135 (2010), pp. 1556–1563 (cit. on p. 4).

[21] F. Banhart J. A. Rodríguez-Manzo C. Pham-Huu. «Graphene growth by a metal-catalyzed solid-state transformation of amorphous carbon». In: *Acs Nano* 5 (2011), pp. 1529–1534 (cit. on p. 4).

[22] I. Lewis. «Chemistry of carbonization». In: *Carbon* 20 (1982), pp. 519–529 (cit. on p. 4).

[23] A. Oberlin. «Carbonization and graphitization». In: *Carbon* 22 (1984), pp. 521–541 (cit. on p. 4).

[24] T. J. Shin B. V. Cunning B. Wang and R. S. Ruoff. «Structure-directing effect of single crystal graphene film on polymer carbonization and graphitization». In: *Materials Orizon* 6 (2019), pp. 796–801 (cit. on p. 4).

[25] a. Morteza-Najarian R. McCreery A. Bergren, S. Y. Sayed, and H. Yan. «Electron transport in all-carbon molecular electronic devices». In: *Faraday discussions* 172 (2014), pp. 9–25 (cit. on p. 5).

[26] R. L. McCreery R. Bowling R. T. Packard. «Mechanism of electrochemical activation of carbon electrodes: role of graphite lattice defects». In: *Langumuir* 5 (1989), pp. 683–688 (cit. on p. 5).

[27] R. L. McCreery R. J. Rice. «Quantitative relationship between electron transfer rate and surface microstructure of laser-modified graphite electrodes». In: *Analytical chemistry* 61 (1989), pp. 1637–1641 (cit. on p. 5).

[28] H. Wu Y. Shao J. Wang, J. Liu, I. A. Aksay, and Y. Lin. «Graphene based electrochemical sensors and biosensors: a review». In: *Electroanalysis: An International Journal Devoted to Fundamental and Practical Aspects of Electroanalysis* 22 (2010), pp. 1027–1036 (cit. on p. 5).

[29] B. J. Venton C. B. Jacobs M. J. Peairs. «Carbon nanotube based electrochemical sensors for biomolecules». In: *Analytica chimica acta* 662 (2010), pp. 105–127 (cit. on p. 5).

[30] X. Jin J.-H. Zhong J. Zhang, J.-Y. Liu, M.-H. Li Q. Li, W. Cai†, D.-Y. Wu, D. Zhan, and B. Ren. «Quantitative correlation between defect density and heterogeneous electron transfer rate of single layer graphene». In: *Journal of the American Chemical Society* 136 (2014), pp. 16609–16617 (cit. on p. 5).

[31] Z. Zhu. «An overview of carbon nanotubes and graphene for biosensing applications». In: *Nano-micro letters* 9.25 (2017) (cit. on p. 5).

[32] G. G. Wildgoose C. E. Banks T. J. Davies and R. G. Compton. «Electrocatalysis at graphite and carbon nanotube modified electrodes: edge-plane sites and tube ends are the reactive sites». In: *Chemical Communications* (2005), pp. 829–841 (cit. on p. 5).

[33] C. Salter C. E. Banks A. Crossley, S. J. Wilkins, and R. G. Compton. «Carbon nanotubes contain metal impurities which are responsible for the "electrocatalysis" seen at some nanotube-modified electrodes». In: *Angewandte Chemie International Edition* 45 (2006), pp. 2533–2537 (cit. on p. 5).

[34] C. E. Banks D. A. Brownson. In: *The handbook of graphene electrochemistry* (2014) (cit. on pp. 5, 13).

[35] Y.-R- Kim A. G. Güell A. S. Cuharuc, G. Zhang, S.-y Tan, N. Ebejer, and P. R. Unwin. «Redox-dependent spatially resolved electrochemistry at graphene and graphite step edges». In: *ACS nano* 9 (2015), pp. 3558–3571 (cit. on p. 5).

[36] B. Narayanan D. Berman S. A. Deshmukh, S. K. R. S. Sankaranarayanan, Z. Yan, A. A. Balandin, A. Zinovev, D. Rosenmann, and A. V. Sumant. «Metal-induced rapid transformation of diamond into single and multilayer graphene on wafer scale». In: *Nature communications* 7 (2016), pp. 1–8 (cit. on p. 5).

[37] D. S. Young A. Moore A. R. J. P. Ubbelohde. «Stress recrystallization of pyrolytic graphite». In: *Proceedings of the Royal Society of London. Series A. Mathematical and Physical Sciences* 280 (1964), pp. 153–169 (cit. on p. 5).

[38] K. Nakamura M. Murakami N. Nishiki, J. Ehara, H. Okada, T. Kouzaki, K. Watanabe, T. Hoshi, and S. Yoshimura. «High-quality and highly oriented graphite block from polycondensation polymer films». In: *Carbon* 30 (1992), pp. 255–262 (cit. on p. 5).

[39] E. H. M. Ferreira L. G. Cançado M. G. da Silva, F. Hof, K. Kampioti, K. Huang, A. Pénicaud, C. A. Achete, R. B. Capaz, and A. Jorio. «Disentangling contributions of point and line defects in the Raman spectra of graphene-related materials». In: *2D Materials* 4.025039 (2017) (cit. on p. 5).

[40] J. Robertson A. C. Ferrari. «Interpretation of Raman spectra of disordered and amorphous carbon». In: *Physical review B* 61.14095 (2000) (cit. on p. 6).

[41] D. M. Basko A. C. Ferrari. «Raman spectroscopy as a versatile tool for studying the properties of graphene». In: *Nature nanotechnology* 8.235 (2013) (cit. on p. 6).

[42] K-D. You E. Cuniberto S-C. Hsu, B. Wu, Z. Huang, X. Pei, and D. Shahrjerdi. «An Electrochemical Biochip for Measuring Low Concentrations of Analytes with Adjustable Temporal Resolutions». In: *IEEE Transactions on Biomedical Circuits and Systems* 14 (2020), pp. 903–917 (cit. on pp. 8, 11–13).

[43] R. M. Wightman J. A. Johnson N. T. Rodeberg. «Measurement of basal neurotransmitter levels using convolution-based nonfaradaic current removal». In: *Analytical Chemistry* 90.12 (2018), pp. 7181–7189 (cit. on p. 11).

[44] J. M. Kita A. Hermans R. B. Keithley, L. A. Sombers, and R. M. Wightman. «Dopamine detection with fast-scan cyclic voltammetry used with analog background subtraction». In: *Analytical Chemistry* 80.11 (2008), pp. 4040–4048 (cit. on p. 11).

[45] S. E. Creager S. D. O'Connor G. T. Olsen. «A Nernstian electron source model for the ac voltammetric response of a reversible surface redox reaction using large-amplitude ac voltages». In: *J. Electroanalytical Chemistry* 466.1 (1999), pp. 197–202 (cit. on p. 11).

[46] J. Leddy A. J. Bard L. R. Faulkner and C. G. Zoski. «Electrochemical Methods: Fundamentals and Applications». In: 2 (1980) (cit. on pp. 12, 23, 24).

[47] G. D. Stuber M. L. A. V. Heien P. E. M. Phillips, A. T. Seipela, and R. M. Wightman. «Overoxidation of carbon-fiber microelectrodes enhances dopamine adsorption and increases sensitivity». In: *Analyst* 128.12 (2003), pp. 1413–1419 (cit. on p. 14).

[48] Q. Cao B.J. Venton. «Fundamentals of fast-scan cyclic voltammetry for dopamine detection». In: *Analyst* 145 (2020), pp. 1158–1168 (cit. on pp. 14, 15).

[49] M. J. Logman P. L. Runnels J. D. Joseph and R. M. Wightman. «Effect of pH and surface functionalities on the cyclic voltammetric responses of carbon-fiber microelectrodes». In: *Analytical Chemistry* 71.14 (1999), pp. 2782–2789 (cit. on p. 15).

[50] R. B. Keithley P. Takmakov M. K. Zachek, E. S. Bucher, G. S. McCarty, and R. M. Wightman. «Characterization of local pH changes in brain using fast-scan cyclic voltammetry with carbon microelectrodes». In: *Analytical Chemistry* 82.23 (2010), pp. 9892–9900 (cit. on p. 15).

[51] M. E. A. Reith J. L. Berfield L. C. Wang. «Which Form of Dopamine Is the Substrate for the Human Dopamine Transporter: the Cationic or the Uncharged Species?» In: *Journal of Biological Chemistry* 274.8 (1999), pp. 4876–4882 (cit. on p. 16).

[52] G. Litwinienko K. Jodko-Piorecka. «First Experimental Evidence of Dopamine Interactions with Negatively Charged Model Biomembranes». In: *ACS Chemical Neuroscience* 4.7 (2013), pp. 1114–1122 (cit. on p. 16).

[53] J. Petrovic P. Hashemi E. C. Dankoski, R. B. Keithley, and R. M. Wightman. «Voltammetric Detection of 5-Hydroxytryptamine Release in the Rat Brain». In: *Analytical Chemistry* 81.22 (2009), pp. 9462–9471 (cit. on p. 17).

[54] K. M. Wood P. Hashemi E. C. Dankoski, R. E. Ambrose, and R. M. Wightman. «In vivo electrochemical evidence for simultaneous 5-HT and histamine release in the rat substantia nigra pars reticulata following medial forebrain bundle stimulation». In: *J. Neurochemistry* 118.5 (2011), pp. 749–759 (cit. on p. 17).

[55] S. M. Dietz B. P. Jackson and R. M. Wightman. «Fast-scan cyclic voltammetry of 5-hydroxytryptamine». In: *Analytical Chemistry* 67.6 (1995), p. 6 (cit. on p. 17).

[56] K. E. Dunham and B. J. Venton. «Improving serotonin fast- scan cyclic voltammetry detection: new waveforms to reduce electrode fouling». In: *Analyst* 145.22 (2020), pp. 7437–7446 (cit. on pp. 17, 18).

[57] M. D. Ward E. Cuniberto Z. Huang and D. Shahrjerdi. «Unraveling the complex electrochemistry of serotonin using engineered graphitic sensors». In: *Analyst* (2022) (cit. on pp. 17, 18).

[58] G. E. Bekhiet A. Radi. «Voltammetry of melatonin at carbon electrodes and determination in capsules». In: *Bioelectrochemistry and Bioenergetics* 45.2 (1998), pp. 275–279 (cit. on pp. 19, 20).

[59] A. E. Ross A. L. Hensley A. R. Colley. «Real-Time Detection of Melatonin Using Fast-Scan Cyclic Voltammetry». In: *Analytical Chemistry* 90 (2018), pp. 8642–8650 (cit. on pp. 19, 20).

[60] M. I. Prodromidis A. C. Lazanas. «Electrochemical Impedance Spectroscopy-A Tutorial». In: *ACS Measurement Science* 3.3 (2023), pp. 162–193 (cit. on pp. 20, 21).

[61] Y. Zhu A.C. Schmidt X. Wang and L.A. Sombers. «Carbon Nanotube Yarn Electrodes for Enhanced Detection of Neurotransmitter Dynamics in Live Brain Tissue». In: *ACS Nano* 7 (2013), pp. 7864–7873 (cit. on p. 23).

[62] B. J. Trafton B. D. Bath D. J. Michael, J. D. Joseph, P. L. Runnels, and R. M. Wightman. «Subsecond adsorption and desorption of dopamine at carbon-fiber microelectrodes». In: *Analytical Chemistry* 72 (2000), pp. 5994–6002 (cit. on p. 24).

[63] R. M. Wightman J. A. Johnson C. N. Hobbs. «Removal of differential capacitive interferences in fast-scan cyclic voltammetry». In: *Analytical Chemistry* 89.11 (2017), pp. 6166–6174 (cit. on p. 25).

[64] R. M. Wightman J. A. Johnson N. T. Rodeberg. «Measurement of basal neurotransmitter levels using convolution-based nonfaradaic current removal». In: *Analytical Chemistry* 90.12 (2018), pp. 7181–7189 (cit. on p. 25).